

# Performance Analysis of Intelligent Reflective Surface Aided Wireless Communications

Dulaj Gunasinghe, *Student Member, IEEE*, Dhanushka Kudathanthirige, *Student Member, IEEE*, and Gayan Amarasuriya Aruma Baduge, *Senior Member, IEEE*

## Abstract

The fundamental performance metrics of an intelligent reflective surface (IRS)-aided wireless system are presented. By optimizing the IRS phase-shift matrix, the received signal-to-noise ratio (SNR) is maximized at the destination in the presence of both reflected and direct channels. The probability distributions of this maximum SNR are tightly approximated for the moderate-to-large reflective element regime. Thereby, the probability density function and cumulative distribution function of this tight SNR approximation are derived in closed-form for Nakagami- $m$  fading to facilitate a statistical characterization of the performance metrics. The outage probability, average symbol error probability, and achievable rate bounds are derived. By virtue of an asymptotic analysis in the high SNR regime, the diversity order is quantified. Thereby, we reveal that the overall diversity order can be scaled as a function of the number of reflective elements ( $N$ ) such that  $G_d = m_v + \min(m_g, m_h)N$ , where  $m_v$ ,  $m_h$  and  $m_g$  are the Nakagami- $m$  parameters of the direct, source-to-IRS and IRS-to-destination channels, respectively. The asymptotic achievable rate is derived, and thereby, it is shown that the transmit power can be scaled inversely proportional to  $N^2$ . The impact of quantized IRS phase-shifts is investigated by deriving the achievable rate bounds. Useful insights are obtained by analyzing the system performance for different severity of fading cases including spatially correlated fading. Our analysis and numerical results reveal that IRS is a promising technology for boosting the performance of wireless communications by intelligently controlling the propagation channels without employing additional active radio-frequency chains.

The authors are with the Department of Electrical and Computer Engineering, Southern Illinois University, Carbondale, IL, USA, Email: {dulaj.gunasinghe,dhanushka.kudathanthirige,gayan.baduge}@siu.edu. This work in part has been presented at IEEE International Conference on Communications (ICC), June, 2020 [1].

## I. INTRODUCTION

Over the past five generations of wireless standards, performance of the transmitter and receiver has been optimized to mitigate various transmission impairments of propagation channels, which are generally assumed to be uncontrollable in the wireless system designer's perspective. However, owing to the recent research advancements of meta-materials and meta-surfaces, a novel concept of coating physical objects such as building walls and windows with intelligent reflective surfaces (IRSs) with reconfigurable reflective properties has been envisioned [1]–[3]. The ultimate goal of IRS is to enable a smart wireless propagation environment by controlling the reflective properties of the underlying channels [3].

An IRS comprises of a very large number of passive reflective elements, which are capable of reconfiguring properties of electromagnetic (EM) waves impinging upon them. On one hand, reflected EM waves can be added constructively at a desired receiver by intelligently controlling phase-shifts at each reflective element to boost the signal-to-noise ratio (SNR) and coverage. On the other hand, a reflected signal can be made to add destructively and thereby to mitigate co-channel interference towards an undesired direction. Moreover, IRS facilitates full-duplex reflections, and hence, large blockages between a pair of transmitter-receiver can be circumvented through smart reflections without trading-off additional time, frequency or power resources. Since an IRS does not generate new EM waves, costly transmit radio-frequency (RF) chains/amplifiers in relays can be eliminated and thereby improving the energy efficiency. Thus, the concept of IRS presents a paradigm shift in wireless communication research.

### A. A literature survey on intelligent reflective surfaces for wireless applications

The fabrication of software-controllable IRS has been shown to be feasible owing to the recent breakthroughs in physics and related fields [4]. The core technical aspects of modeling IRS to enable reconfigurable EM properties are currently being developed [2]. The prototypes of meta-surfaces and meta-tiles with artificial thin-film of EM materials, which are intended to coat physical objects to enable a smart wireless environment, are being developed [4].

Recently, several attempts of adopting IRS into wireless system designs have been reported [5]–[20]. The joint precoder and IRS phase-shift optimization techniques to maximize the received SNR are investigated in [5] for a multi-antenna transmitter in the presence of an IRS. Reference [6] adopts basic ray tracing techniques to model multi-path propagation through an IRS, and thereby, authors propose transmission strategies to control the reflections by virtue of phase-shift optimization at passive elements embedded within an IRS. In [10], joint IRS

and beamforming optimization is studied with a practical phase-shift model. Reference [7] proposes an efficient phase-shift optimization design based on maximizing an upper bound of the average spectral efficiency of the IRS-aided communications. The smart propagations enabled by an IRS have been exploited in [8] to boost the physical layer security. In [9], the impact of having a limited number of phase-shifts at the IRS and the corresponding phase-shift designs are investigated. In [11], the asymptotic achievable uplink rate is derived by adopting the channel hardening effects for very large reflective element regime. Reference [12] investigates optimization techniques to maximize the signal-to-interference-plus-noise ratio (SINR) of an IRS-aided communication between a multi antenna base-station (BS) and single-antenna users. In [13], the outage probability is studied for multiple IRS-aided wireless systems. In [14], the asymptotic rate distribution of the IRS-aided systems operating in Rician fading is derived. In [15], the IRS-based communication with phase-shift errors is investigated, and it has been shown that the cascaded channel through an IRS with phase errors is equivalent to a point-to-point channel with Nakagami fading. The performance of a random rotation-based IRS communication is studied in [16] by proposing four low-complexity and energy efficient techniques via the coding- and selection-based approaches. In [17], the maximal ratio transmission precoder is used at the BS to facilitate IRS-based communication with single-antenna users, and thereby, the outage probability minimization is performed by optimizing the IRS phase-shifts. In [18], the authors have shown that the multi-path fading and the related Doppler effects caused by the relative movement of the mobile nodes can be mitigated by real-time adjustable IRS phase-shifts. In [18], a number of design trade-offs between the fade pattern elimination and complex envelope magnitude maximization has been investigated. In [21], the impact of distributed IRS deployments is studied. In [19], it has been shown that when compared with the two-dimensional (2D) IRS, the spherical IRS has several advantages such as wider coverage, simpler positioning technique and flexible deployment. In [20], the capacity region of an IRS-aided two user multiple access channel has been characterized for distributed and centralized IRS deployment, and thereby, it has been shown that centralized deployment outperforms the distributed counterpart.

This paper goes beyond our related conference paper [1] by presenting the performance metrics with the direct channel, Nakagami- $m$  fading, asymptotic analysis in large reflective element regime, transmit power scaling laws, and impact of phase-shift quantization. In [1], Rayleigh fading has been considered, and the outage probability, average symbol error rate (SER) and achievable rate of the IRS reflected channel (without the direct channel) have been derived.

### B. Motivation and our contribution

The main contribution of this paper is to present a closed-form performance analysis for IRS-aided wireless systems operating over Nakagami- $m$  fading. The key idea of an IRS is to enable a programmable control over the wireless propagation channels. This necessitates innovations of radically novel techniques for modeling, designing and analyzing wireless systems as the resulting smart propagation channels can now be able to interact with EM waves impinging upon them in a software-controlled manner. Although several important attempts have recently been made [2]–[9], [11]–[20], the fundamental research on IRS in wireless communication’s perspective is still at an embryonic stage. For instance, a mathematically tractable statistical characterization of the optimal end-to-end SNR that is attainable via an IRS-aided reflections and direct channel over Nakagami- $m$  fading has not yet been investigated. Specifically, Nakagami- $m$  fading model is versatile in the sense that it can model a wide-range of multi-path fading environments [22]. For instance,  $m = 1/2$  captures the most severe fading with a one-sided Gaussian distribution, while  $m = 1$  models the Rayleigh fading with rich-scattering. When  $m \approx (K + 1)^2/(2K + 1)$ , Nakagami- $m$  fading can be used to approximate Rician fading, where  $K$  is the Rician factor [22]. It can also capture less severe fading cases when  $m$  is large. Moreover, insightful closed-form analyses on the outage probability, average SER, achievable rate, diversity order and array gain have not yet been reported to IRS-aided communications in the presence of the direct channel. The detrimental impact of phase-shift quantizations at the IRS elements has not yet been analytically quantified into the above performance metrics. The above facts and the important research gaps have motivated the current work. To this end, our paper presents a comprehensive performance analysis framework for deriving the fundamental bounds pertaining to an IRS intended for aiding the end-to-end communication between a single-antenna source ( $S$ ) and a destination ( $D$ ). The distinct contribution of this work can be summarized as follows:

- 1) We statistically characterize the received SNR that is attainable by virtue of optimal phase-shift control at the IRS elements such that all reflected channels are constructively combined with the direct channel. To this end, the probability density function (PDF) and cumulative function (CDF) of a tight approximation of the optimal SNR are derived in closed-form for Nakagami- $m$  fading. We reveal that this statistical characterization is mathematically tractable to facilitate the closed-form derivations of important performance metrics, and the resulting PDF/CDF approximations are significantly tight to the exact counterparts in the moderate-to-large reflective element regime.

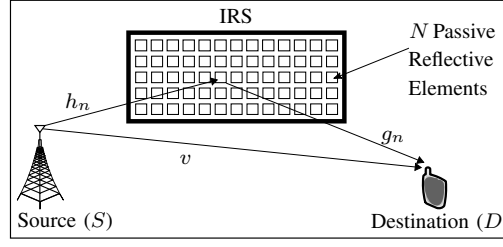


Fig. 1. An IRS-aided wireless set-up. The distances  $S$ - $D$ ,  $S$ -IRS, and  $D$ -IRS are denoted by  $d_{SD}$ ,  $d_{SI}$ , and  $d_{DI}$ , respectively.

- 2) By using our PDF/CDF analysis, novel, tight approximations/bounds for the outage probability, average SER, and achievable rate are derived in closed-form. Thereby, useful design insights are obtained. By using the asymptotic outage probability and average SER analyses in the high SNR regime, the diversity order and array/coding gain are quantified. This asymptotic analysis reveals that the diversity order is an affine function of the number of IRS elements ( $N$ ), and hence, the system reliability metrics such as the outage probability and average SER can be boosted merely by virtue of passive reflections of exiting EM waves without adopting to costly/active RF chains. Moreover, we derive the asymptotic achievable rate in the large reflective element regime ( $N \rightarrow \infty$ ), and thereby, we reveal that the our lower and upper rate bounds are asymptotically exact as  $N \rightarrow \infty$ . Specifically, we show that the transmit power can be scaled inversely proportional to the square of the number of IRS elements in the asymptotic  $N$  regime, while achieving a finite rate.
- 3) Finally, we discuss the practical design aspects and draw insights via our analysis. In this context, we investigate the impact of hardware-limited quantized phase-shifts at the IRS elements. The underlying deleterious effects are analytically quantified by deriving the outage probability and achievable rate bounds. Thereby, we reveal that the quantized IRS phase-shifts considerably hinder the system performance compared to the continuous phase-shifts. Further, we show that our analysis can be used to deduce performance metrics for distinctly asymmetric fading cases including, the most severe one-sided Gaussian, Rayleigh/rich-scattering, unserviceable direct channel, and less severe multi-path fading. Moreover, the impact of spatially correlated fading is studied.

**Notation:**  $\mathbb{E}[X]$  and  $\mathbb{V}\text{ar}[X]$  are the expectation and variance of a random variable (RV)  $X$ , respectively.  $X \sim \mathcal{N}(\mu_X, \sigma_X^2)$  denotes that  $X$  is Gaussian distributed with  $\mu_X$  mean and  $\sigma_X^2$  variance.  $\Gamma(z) = \int_0^\infty e^{-t} t^{z-1} dt$  is the Gamma function [23, 8.310.1].  $\Gamma(q, z) = \int_z^\infty t^{q-1} e^{-t} dt$  [23, 8.350.2] and  $\gamma(q, z) = \int_0^z t^{q-1} e^{-t} dt$  [23, 8.350.1] are the upper and lower incomplete Gamma functions, respectively.  $\mathcal{O}(z^p)$  denotes the remainder in a Maclaurin series [23, 0.318.2] after the  $z^p$  term, and  $\otimes$  denotes the Kronecker product.

## II. SYSTEM, CHANNEL AND SIGNAL MODELS

### A. System and channel models

We consider an IRS-assisted communication system in which a source ( $S$ ) communicates with a destination ( $D$ ) via an IRS (Fig. 1). The  $S$  and  $D$  are single-antenna nodes, while the IRS is embedded with  $N$ -passive reflective elements. The IRS is able to control the phase-shifts of incident/impinging EM waves such that the received signals can be constructively combined at  $D$ , while the reflected signal amplitudes are also attenuated. Thus, the reflective coefficient of the  $n$ th IRS element can be modeled as  $r_n = \eta_n e^{j\theta_n}$ , where  $0 < \eta_n \leq 1$  and  $-\pi < \theta_n \leq \pi$  are amplitude attenuation coefficient and phase-shift, respectively, for  $1 \leq n \leq N$ .

The channels from  $S$  to  $D$ ,  $S$  to the  $n$ th element of IRS, and the  $n$ th IRS element to  $D$  are denoted by  $v$ ,  $h_n$  and  $g_n$ , respectively, where  $1 \leq n \leq N$ . These complex channel coefficients can be written in polar form as  $v = \bar{v} \exp(j\phi_v)$ ,  $h_n = \bar{h}_n \exp(j\phi_{h_n})$ , and  $g_n = \bar{g}_n \exp(j\phi_{g_n})$ , where  $\{\bar{v}, \bar{h}_n, \bar{g}_n\}$  and  $\{\phi_v, \phi_{h_n}, \phi_{g_n}\}$  are the channel amplitudes/envelopes and phases of the respective channels. To represent a wide range of fading scenarios, we adopt Nakagami- $m$  channel fading model. Therefore, the PDF of  $\bar{v}$  is given by

$$f_{\bar{v}}(x) = \frac{2m_v^{m_v} x^{2m_v-1}}{\Gamma(m_v) \kappa_v^{m_v}} \exp\left(-\frac{m_v x^2}{\kappa_v}\right) \text{ for } x \geq 0, \quad (1)$$

where  $m_v$  and  $\kappa_v = m_v \zeta_v$ , respectively, denote the shape and scaling parameters of the Nakagami- $m$  distribution [24]. Here,  $\zeta_v$  captures the large-scale fading of the channel. Similarly, the PDFs of  $\bar{g}_n$  and  $\bar{h}_n$  can be readily obtained by replacing  $m_v$  and  $\kappa_v = m_v \zeta_v$  in (1) by the corresponding channel parameters;  $\{m_g \text{ and } \kappa_g = m_g \zeta_g\}$  and  $\{m_h \text{ and } \kappa_h = m_h \zeta_h\}$ .

### B. Signal model

The signal received at  $D$  via the direct and IRS-aided reflected channels can be written as [5]

$$r = \sqrt{p} v x + \sqrt{p} \sum_{n=1}^N g_n \eta_n \exp(j\theta_n) h_n x + n, \quad (2)$$

where  $p$  is transmit power, and  $x$  is transmitted signal at  $S$ , satisfying  $\mathbb{E}[|x|^2] = 1$ . Moreover,  $n$  is an additive white Gaussian noise (AWGN) at  $D$  with zero mean and variance  $\sigma^2$  such that  $n \sim \mathcal{CN}(0, \sigma^2)$ . In (2), the first and second components account for the received signal via the direct channel and IRS-aided reflected channel, respectively. By replacing  $v$ ,  $h_n$ , and  $g_n$  by their polar forms presented in Section II-A, the received SNR at  $D$  can be derived by using (2) as

$$\tilde{\gamma} = \bar{\gamma} \left| \bar{v} \exp(j\phi_v) + \sum_{n=1}^N \bar{g}_n \bar{h}_n \eta_n \exp([j(\phi_{g_n} + \phi_{h_n} + \theta_n)]) \right|^2, \quad (3)$$

where  $\bar{\gamma} = p/\sigma^2$  is defined as the transmit SNR.

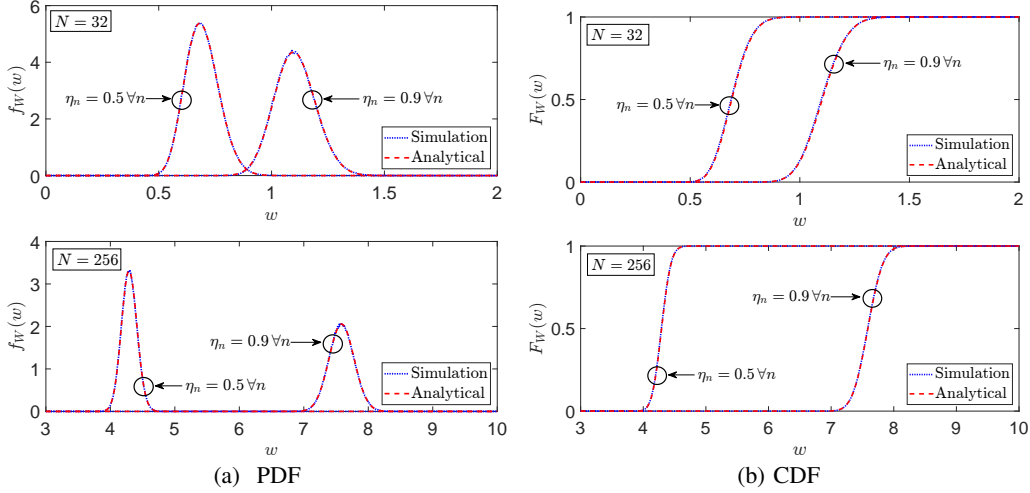


Fig. 2. The exact PDF and CDF of  $\tilde{W} = \sum_{n=1}^N \bar{g}_n \bar{h}_n \eta_n$  via Monte-Carlo simulations and our analysis (7) and (8).

**Lemma 1:** *The maximum received SNR at  $D$  that can be attained by controlling the phase-shifts at the IRS elements is given by*

$$\tilde{\gamma}^* = \bar{\gamma} \left| \bar{v} + \sum_{n=1}^N \bar{g}_n \bar{h}_n \eta_n \right|^2, \quad (4)$$

and the corresponding optimal phase-shifts are given by

$$\theta_n^* = \phi_v - (\phi_{h_n} + \phi_{g_n}), \quad \text{for } 1 \leq n \leq N. \quad (5)$$

*Proof.* The signals received at  $D$  via the IRS-aided reflected channel or equivalently  $N$  terms inside the summation of (3) must be constructively added to the signal received via the direct channel to maximize the received SNR at  $D$ . This can be accomplished by controlling the phase-shift of each IRS element ( $\theta_n$ ) to match the phase of the direct channel ( $\phi_v$ ), i.e.,  $\phi_v = \phi_{g_n} + \phi_{h_n} + \theta_n$ ,  $\forall n$ . Thereby, the optimal phase-shift at the  $n$ th IRS element can be derived as shown in (5). By substituting (5) into (3), the maximum SNR at  $D$  can be derived as (4).  $\square$

### III. PERFORMANCE ANALYSIS

#### A. Statistical characterization of the optimal received SNR

To begin with, we derive a tight approximation for  $\tilde{\gamma}^*$  in (4). To begin with, we notice that

$$\tilde{W} = \sum_{n=1}^N \bar{g}_n \bar{h}_n \eta_n \quad (6)$$

is a sum of the products of independent Nakagami distributed RVs  $\bar{g}_n$  and  $\bar{h}_n$  for  $n \in \{1, \dots, N\}$ . The derivation of the exact probability distribution of  $\tilde{W}$  is mathematically involved and may not provide useful technical insights. Thus, we resort to tight approximations to facilitate a mathematically tractable performance analysis. To this end, by invoking the central limit theorem (CLT) [24],  $\tilde{W}$  in (6) can be tightly approximated by  $W$ , whose PDF and CDF are presented in Lemma 2.

**Lemma 2:** For a sufficiently large number of reflective elements, the PDF and CDF of  $W$  are given by

$$f_W(w) = \frac{\xi}{\sqrt{2\pi\bar{\sigma}}} \exp(-(w - \bar{\mu})^2/2\bar{\sigma}^2) \quad \text{for } w \geq 0 \text{ and } 0 \text{ otherwise,} \quad (7)$$

$$F_W(w) = 1 - \xi \mathcal{Q}\left((w - \bar{\mu})/\bar{\sigma}\right) \quad \text{for } w \geq 0 \text{ and } 0 \text{ otherwise,} \quad (8)$$

where the parameters  $\bar{\mu}$  and  $\bar{\sigma}^2$  can be defined as

$$\bar{\mu} = \sum_{n=1}^N \eta_n \sqrt{\frac{\kappa_{g_n} \kappa_{h_n}}{m_g m_h}} T(m_g, m_h, 1/2), \quad \text{and} \quad \bar{\sigma}^2 = \sum_{n=1}^N \eta_n^2 \kappa_{g_n} \kappa_{h_n} \left(1 - \frac{T^2(m_g, m_h, 1/2)}{m_g m_h}\right), \quad (9)$$

where  $T(a, b, i) = \Gamma(a+i)\Gamma(b+i)/(\Gamma(a)\Gamma(b))$ , and  $\mathcal{Q}(\cdot)$  denotes the Gaussian- $\mathcal{Q}$  function with  $\xi = 1/\mathcal{Q}(\bar{Z})$  and  $\bar{Z} = -\bar{\mu}/\bar{\sigma}$ .

*Proof.* See Appendix A. □

**Remark 1:** The accuracy of Lemma 2 is verified via Monte-Carlo simulations in Fig. 2a and Fig. 2b, where our analytical PDF and CDF of  $W$  in (7) and (8) are plotted for different  $N$  values. These figures reveal that our analytical PDF and CDF are significantly tight to the exact Monte-Carlo simulations even for moderately large  $N$  values.

**Remark 2:** By using Lemma 2, it can be shown that as  $N$  grows without bound, the mean and variance of  $W$  indeed approach  $\bar{\mu}$  and  $\bar{\sigma}^2$  in (9). To prove this, we first derive the mean and variance of  $W$  by using the PDF in (7) as follows [24]:

$$\mu_W = \bar{\mu} + \bar{\sigma} \xi \phi(\bar{Z}) \quad \text{and} \quad \sigma_W^2 = \bar{\sigma}^2 (1 + \bar{Z} \xi \phi(\bar{Z}) - (\xi \phi(\bar{Z}))^2), \quad (10)$$

where  $\phi(x) = e^{-x^2/2}/\sqrt{2\pi}$ . Then the asymptotic values of (10) are given by

$$\lim_{N \rightarrow \infty} \mu_W - \bar{\mu} \rightarrow 0 \quad \text{and} \quad \lim_{N \rightarrow \infty} \sigma_W^2 - \bar{\sigma}^2 \rightarrow 0. \quad (11)$$

*Proof.* When  $N$  grows large, by invoking the fact that

$$\lim_{N \rightarrow \infty} \left( \sum_{n=1}^N x_n \right) / \sqrt{\sum_{n=1}^N x_n^2} \rightarrow \infty, \quad (12)$$

where  $x_n = \eta_n \sqrt{\kappa_{g_n} \kappa_{h_n}}$ , we can readily show that  $\bar{Z} = -\bar{\mu}/\bar{\sigma} \rightarrow -\infty$ , where  $\bar{Z}$  is a parameter in (10). Then, these results hold;  $\phi(\bar{Z}) \xrightarrow{N \rightarrow \infty} 0$ ,  $\bar{Z} \phi(\bar{Z}) \xrightarrow{N \rightarrow \infty} 0$ , and  $\xi \xrightarrow{N \rightarrow \infty} 1$ . By substituting these asymptotic values into (10), the desired result can be derived as shown in (11). □

**Remark 3:** The IRSs are meant to be installed on walls, ceilings, building facades, and advertisement panels [25]. They are comprised of low profiles with conformal geometry and light weight, and thus, they are cost effective [26]. Thus, IRSs with moderate to large number of reflective elements ( $N$ ) are a feasible assumption in terms of space requirements and cost.



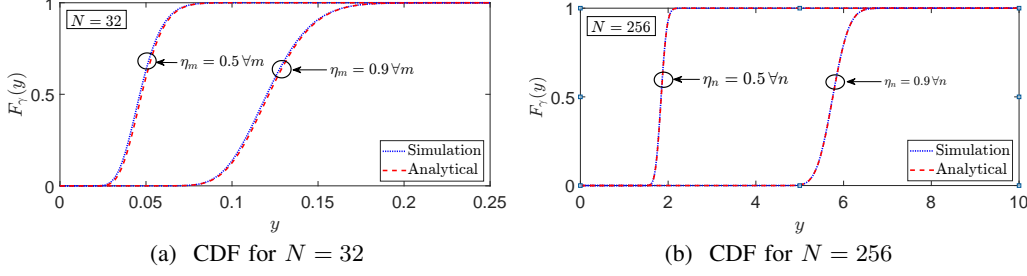


Fig. 3. The exact CDF of  $\tilde{\gamma}^*$  via Monte-Carlo simulations and its analytical approximation  $F_\gamma(y)$  in (14).

By using Lemma 2, a tight approximation for the optimal received SNR ( $\tilde{\gamma}^*$ ) is derived as

$$\tilde{\gamma}^* \approx \gamma = \bar{\gamma} |\bar{v} + W|^2, \quad (13)$$

where  $W$  is our proposed tight approximation to  $\tilde{W}$  in (6). Next, the CDF of  $\gamma$  is derived as

$$F_\gamma(y) = \begin{cases} 2\lambda\sqrt{a\bar{\sigma}^2} \sum_{k=0}^{\tilde{m}_v-k} \binom{\tilde{m}_v-k}{k} (-1)^{\tilde{m}_v-k} \left[ \mathcal{J}\left(k, \frac{\bar{\mu}}{2\sqrt{a\bar{\sigma}^2}}\right) - \mathcal{J}\left(k, \frac{\bar{\mu} - \sqrt{y/\bar{\gamma}}}{2\sqrt{a\bar{\sigma}^2}}\right) \right], & 0 < y \leq \bar{\gamma}\bar{\mu}^2 \\ 1 - 2\lambda\sqrt{a\bar{\sigma}^2} \sum_{k=0}^{\tilde{m}_v-k} \binom{\tilde{m}_v-k}{k} \left[ [(-1)^k + 1] \Gamma\left(\frac{k+1}{2}\right) \mathcal{I}\left(k, \frac{\sqrt{y/\bar{\gamma}} - \bar{\mu}}{2\sqrt{a\bar{\sigma}^2}}\right) \right. \\ \quad \left. + \mathcal{J}\left(k, \frac{\sqrt{y/\bar{\gamma}} - \bar{\mu}}{2\sqrt{a\bar{\sigma}^2}}\right) \right], & y > \bar{\gamma}\bar{\mu}^2, \end{cases} \quad (14)$$

and 0 otherwise. In (14),  $\tilde{m}_v$ ,  $a$ ,  $\lambda$  and can be defined as

$$\tilde{m}_v = 2m_v - 1, \quad a = m_v/\kappa_v + 1/(2\bar{\sigma}^2) \quad \text{and} \quad \lambda = m_v^{m_v} \xi / \left( \Gamma(m_v) \kappa_v^{m_v} a^{m_v} \sqrt{2\pi\bar{\sigma}^2} \right), \quad (15)$$

where  $\bar{\mu}$  and  $\bar{\sigma}^2$  are defined in (10). In (14),  $\mathcal{J}(k, x)$  for  $x \geq 0$  and  $\mathcal{I}(k, x)$  can be defined as

$$\mathcal{J}(k, x) = \begin{cases} \mathcal{J}_o(k, x), & \text{for } k = 2t + 1, t \in \mathbb{Z}, \\ \mathcal{J}_e(k, x), & \text{for } k = 2t, t \in \mathbb{Z} \cup \{0\}, \end{cases} \quad (16)$$

$$\mathcal{I}(k, x) = \frac{1}{2} \Gamma\left(\frac{k+1}{2}\right) + \frac{1}{2} (-1)^k \gamma\left(\frac{k+1}{2}, x^2\right) \quad \text{for } x < 0, \quad (17)$$

and  $\mathcal{I}(k, x) = \Gamma\left(\frac{k+1}{2}, x^2\right)/2$  for  $x \geq 0$ . In (16),  $\mathcal{J}_o(k, x)$  and  $\mathcal{J}_e(k, x)$  can be defined as

$$\mathcal{J}_o(k, x) = \frac{(\delta_o - 1)!}{2} \sum_{i=0}^{\delta_o-1} \frac{1}{i! (2\bar{\sigma}^2 a)^{\delta_o+i}} \Gamma\left(m_v + i - \frac{k}{2}, 2\bar{\sigma}^2 a x^2\right), \quad (18a)$$

$$\mathcal{J}_e(k, x) = \sum_{j=0}^{\delta_e-1} \frac{(\delta_e - 1)!}{2(\Delta)^{\delta_e-j} j!} \left[ x^{2j} e^{-\Delta x^2} \Gamma(k', x^2) - \frac{1}{(2\bar{\sigma}^2 a)^{k'+j}} \Gamma(k' + j, 2\bar{\sigma}^2 a x^2) \right], \quad (18b)$$

where  $\delta_o = (k+1)/2$ ,  $\delta_e = m_v - k/2$ ,  $k' = (k+1)/2$ , and  $\Delta = 2\bar{\sigma}^2 a - 1$ .

The PDF of  $\gamma$  is given by  $f_\gamma(y) = f_R(\sqrt{y/\bar{\gamma}})/(2\sqrt{y\bar{\gamma}})$ , where  $f_R(x)$  is defined in (57).

*Proof.* See Appendix B.  $\square$

**Remark 4:** The tightness of our approximated CDF of the optimal SNR (14) derived via (13) is validated in Fig. 3. Here, we plot our analytical CDF (14) for different  $N$  and  $\eta_n$ , and it is compared against the exact CDF of the optimal SNR ( $\tilde{\gamma}^*$ ) via Monte-Carlo simulations. Fig. 3 reveals that our analytical CDF is accurate even for a moderately large number of IRS elements ( $N = 32$ ), and this tightness significantly improves for the high  $N$  regime ( $N = 256$ ). Thus, this observation verifies that our approximated yet tractable statistical characterization is accurate.

### B. Outage probability

The SNR outage probability is defined as the probability that the instantaneous SNR ( $\tilde{\gamma}$ ) falls below a threshold SNR<sup>1</sup> ( $\gamma_{th}$ ). By using (13), a tight approximation to the outage probability for the moderately large  $N$  regime can be written as

$$P_{out} = P_r(\tilde{\gamma}^* \leq \gamma_{th}) \approx F_\gamma(\gamma_{th}), \quad (19)$$

where  $F_\gamma(\cdot)$  is given in (14).

**Remark 5:** To obtain insights, we investigate the asymptotic outage probability in high SNR regime. The analytical behavior of outage probability (19) in high SNR regime can be given by

$$\lim_{\tilde{\gamma} \rightarrow \infty} P_{out} = P_{out}^\infty \approx (O_c \tilde{\gamma})^{-G_d} + \mathcal{O}(\tilde{\gamma}^{-(G_d+1)}), \quad (20)$$

where  $G_d$  is the achievable diversity order, and  $O_c$  is a measure of the array gain [27]. By deriving a single-polynomial approximation for  $P_{out}$ , the asymptotic outage probability can be derived as presented in Theorem 1.

*Theorem 1: For the case of  $m_h \neq m_g$ , when  $\tilde{\gamma} \rightarrow \infty$ , the asymptotic outage probability can be derived as*

$$P_{out}^\infty = \Omega_{op} (\gamma_{th}/\tilde{\gamma})^{G_d} + \mathcal{O}((\gamma_{th}/\tilde{\gamma})^{(G_d+1)}), \quad (21)$$

where the diversity order  $G_d$  is given by

$$G_d = m_v + \min(m_g, m_h)N. \quad (22)$$

In (21),  $\Omega_{op}$  is given by

$$\Omega_{op} = \frac{2m_v^{m_v} \Gamma(2m_v)}{\Gamma(m_v) \kappa_v^{m_v}} \left[ \frac{4(m_a m_b)^{m_c} \Gamma(2m_c + \frac{1}{2}) \Gamma(2m_b - 2m_a - 1)}{\Gamma(m_a) \Gamma(m_b) \Gamma(m_b - m_a + \frac{1}{2}) \Gamma(2m_b)} \right]^N \left( \prod_{n=1}^N \frac{1}{\sqrt{\eta_n^2 \kappa_a \kappa_b}} \right)^{m_c}, \quad (23)$$

where  $m_a = \min(m_g, m_h)$ ,  $m_b = \max(m_g, m_h)$ , and  $m_c = (m_a + m_b)/2$ . Further,  $\kappa_a$  and  $\kappa_b$  are scaling parameters of the corresponding channels. Moreover, the asymptotic array gain ( $O_c$ ) in (20) is given by  $O_c = \gamma_{th}^{-1} \Omega_{op}^{-1/G_p}$ . When  $m_g = m_h = m$ , the diversity order reduces (22) to  $G_d = m_v + mN$ . This confirms that the achievable diversity order can be linearly increased with the number of passive IRS elements without employing any additional active RF chains.

*Proof.* See Appendix C.  $\square$

**Remark 6:** Our asymptotic outage analysis reveals that the diversity order is an affine/linear function of the number of passive reflective elements ( $N$ ). It is noteworthy to mention that this diversity gain is achieved without employing active RF chains at the IRS and in the presence of single-antenna  $S$ - $D$  pair. The diversity order of the direct transmission between  $S$  and  $D$  is

<sup>1</sup>The rate outage probability can be defined as  $P_r(\mathcal{R} = \log_2(1 + \gamma) \leq \mathcal{R}_{th})$ , where  $\mathcal{R}$  and  $\mathcal{R}_{th}$  are the achievable rate and a threshold, respectively. Thus, it is readily related to the SNR outage probability;  $P_r(\gamma \leq 2^{\mathcal{R}_{th}} - 1)$ .

$G_d = m_v$ , where  $m_v$  is the Nakagami- $m$  parameter of the direct channel. Thus, the IRS-aided system achieves an additional diversity gain of  $\min(m_g, m_h)N$ , which is directly proportional to  $N$ . Thus, this diversity gain is attainable by recycling the existing EM waves via passive reflections without generating new EM waves from active RF chains. This diversity gain directly translates into reliability improvements in terms of outage probability and average SER. Thus, the system performance can be boosted via constructive signal combining at  $D$  by virtue of intelligently controllable phases-shifts of passive reflective elements at the IRS.

### C. Average achievable rate

The average achievable rate can be defined as

$$\mathcal{R} = \mathbb{E}[\log_2(1 + \tilde{\gamma}^*)] \approx \mathbb{E}[\log_2(1 + \gamma)], \quad (24)$$

where  $\gamma$  is given in (13). Since the exact derivation of the expectation in (24) is mathematically involved, we derive tight upper and lower bounds by invoking Jensen's inequality as  $\mathcal{R}_{lb} \leq \mathcal{R} \leq \mathcal{R}_{ub}$  [28], where  $\mathcal{R}_{lb}$  and  $\mathcal{R}_{ub}$  are defined as

$$\mathcal{R}_{lb} = \log_2(1 + (\mathbb{E}[1/\gamma])^{-1}) \quad \text{and} \quad \mathcal{R}_{ub} = \log_2(1 + \mathbb{E}[\gamma]). \quad (25)$$

*Theorem 2: By evaluating the expectations in (25), the tight achievable rate lower and upper bounds can be derived in closed-form as*

$$\mathcal{R}_{lb} = \log_2 \left( 1 + \frac{\bar{\gamma} \left( \kappa_v + 2\mu_W \Gamma(m_v + 1/2) \sqrt{\kappa_v/m_v} / \Gamma(m_v) + \mu_W^2 + \sigma_W^2 \right)^3}{\frac{\xi}{2\sqrt{\pi}} \left[ \sum_{k=0}^4 \binom{4}{k} \frac{\Gamma(m_v + k/2)}{\Gamma(m_v)} \left( \frac{\kappa_v}{m_v} \right)^{k/2} \sum_{i=0}^{4-k} \binom{4-k}{i} (2\bar{\sigma}^2)^{i/2} \bar{\mu}^{4-k-i} \mathcal{I} \left( i, \frac{-\bar{\mu}}{\sqrt{2\bar{\sigma}^2}} \right) \right]} \right), \quad (26)$$

$$\mathcal{R}_{ub} = \log_2 \left( 1 + \bar{\gamma} \left( \kappa_v + 2\mu_W \Gamma(m_v + 1/2) \sqrt{\kappa_v/m_v} / \Gamma(m_v) + \mu_W^2 + \sigma_W^2 \right) \right), \quad (27)$$

where  $\mathcal{I}(k, x)$  is defined in (17).

*Proof.* See Appendix D. □

1) *Asymptotic achievable rate when  $N \rightarrow \infty$ :* To obtain further insights, we derive the asymptotic rate when the number of reflective elements grows without bound. As per our achievable rate analysis in Section III-C, in the asymptotic  $N$  regime, the source transmit power ( $p$ ) can be scaled inversely proportional to the square of the number of IRS elements ( $N$ ). Thus, by scaling the transmit power at  $S$  as  $E = p/N^2$ , we show that the upper and lower bounds of the achievable rate converge to a common asymptotic value when the number of IRS elements grows without bound as follows:

$$\lim_{N \rightarrow \infty} \mathcal{R}_{lb} = \mathcal{R}^\infty \quad \text{and} \quad \lim_{N \rightarrow \infty} \mathcal{R}_{ub} = \mathcal{R}^\infty, \quad (28)$$

where the asymptotic rate  $\mathcal{R}^\infty$  in the limit of infinitely many IRS elements is given by

$$\mathcal{R}^\infty = \log_2 \left( 1 + \bar{\gamma}_E \eta^2 \kappa_g \kappa_h T(m_g, m_h, 1/2) / (m_g m_h) \right), \quad (29)$$

where  $\bar{\gamma}_E = E/\sigma_n^2$ . This result also confirms that our achievable rate lower and upper bounds in (26) and (27) are asymptotically exact.

*Proof.* See Appendix D.  $\square$

#### D. Average symbol error rate (SER)

The average SER is defined as the expectation of the conditional error probability ( $P_{e|\tilde{\gamma}^*}$ ) over the distribution of  $\tilde{\gamma}^*$  [29]. For a wide-range of modulation schemes,  $P_{e|\tilde{\gamma}^*}$  is given by  $P_{e|\tilde{\gamma}^*} = \alpha \mathcal{Q}(\sqrt{\beta \tilde{\gamma}^*})$ , where  $\alpha$  and  $\beta$  are modulation dependent parameters [29]. For instance,  $(\alpha, \beta)$  for binary shift-keying (BPSK) and  $M$ -ary quadrature amplitude modulation (QAM) can be defined as  $(1, 2)$  and  $(4(\sqrt{M} - 1)/\sqrt{M}, 3/(M - 1))$ , respectively [30]. Then, the average SER can be derived as  $\bar{P}_e = \mathbb{E}[\alpha \mathcal{Q}(\sqrt{\beta \tilde{\gamma}^*})]$ . By using (13),  $\bar{P}_e$  can be tightly approximated as

$$\bar{P}_e \approx \mathbb{E} \left[ \alpha \mathcal{Q} \left( \sqrt{\beta \tilde{\gamma}} (\bar{v} + W) \right) \right]. \quad (30)$$

*Theorem 3:* An upper bound for  $\bar{P}_e$  can be derived as

$$\bar{P}_e \leq \frac{\alpha \xi m_v^{m_v} \exp\left(-\frac{\bar{\mu}^2}{2\bar{\sigma}^2}\right)}{\kappa_v^{m_v} \sqrt{2\bar{\sigma}^2}} \frac{\exp\left(\bar{\mu}^2 \left[2\bar{\sigma}^2 + \frac{2\beta\bar{\gamma}\bar{\sigma}^4}{\cos^2(\vartheta_u)}\right]^{-1}\right)}{\left(\frac{m_v}{\kappa_v} + \frac{\beta\bar{\gamma}}{2\sin^2(\vartheta_u)}\right)^{m_v} \sqrt{\frac{1}{2\bar{\sigma}^2} + \frac{\beta\bar{\gamma}}{2\cos^2(\vartheta_u)}}} \mathcal{Q}\left(-\frac{\sqrt{2}\bar{\mu}}{1 + \frac{\beta\bar{\gamma}\bar{\sigma}^2}{\cos^2(\vartheta_u)}}\right), \quad (31)$$

where  $\vartheta_u$  is given by

$$\vartheta_u = \operatorname{argmax}_{0 \leq \vartheta \leq \pi/2} \left[ \bar{\mu}^2 \left( 2\bar{\sigma}^2 + \frac{2\beta\bar{\gamma}\bar{\sigma}^4}{\cos^2(\vartheta)} \right)^{-1} - m_v \ln \left( \frac{m_v}{\kappa_v} + \frac{\beta\bar{\gamma}}{2\sin^2(\vartheta)} \right) - \frac{1}{2} \ln \left( \frac{1}{2\bar{\sigma}^2} + \frac{\beta\bar{\gamma}}{2\cos^2(\vartheta)} \right) + \ln \left( \mathcal{Q} \left( -\frac{\sqrt{2}\bar{\mu}}{1 + \frac{\beta\bar{\gamma}\bar{\sigma}^2}{\cos^2(\vartheta)}} \right) \right) \right]. \quad (32)$$

*Proof.* See Appendix E.  $\square$

**Remark 7:** In order to draw useful insights, we derive the asymptotic average SER in the high SNR regime. Thereby, we show that the achievable diversity order is same as that resulted from the asymptotic outage probability analysis in (21). Moreover, the coding gain is also quantified. Thus, the asymptotic average SER is presented in Theorem 3.

*Theorem 3:* When  $m_h \neq m_g$ , the asymptotic SER as  $\bar{\gamma} \rightarrow \infty$  can be derived as

$$P_e^\infty = (G_c \bar{\gamma})^{-G_d} + \mathcal{O}(\bar{\gamma}^{-(G_d+1)}), \quad (33)$$

where the diversity order ( $G_d$ ) is same as (22);  $G_d = m_v + \min(m_g, m_h)N$ , and the array/coding gain ( $G_c$ ) is given by  $G_c = \beta(\alpha 2^{G_d-1} \Omega_{op} \Gamma(G_d + 1/2)/\sqrt{\pi})^{-1/G_d}$ , where  $\Omega_{op}$  is defined in (23).

*Proof.* See Appendix C.  $\square$

#### IV. EFFECTS OF QUANTIZED PHASE-SHIFTS

In the previous section, we assumed that the IRS elements are capable of providing continuous phase-shifts as defined by  $\theta_n^* \forall n$  in (5). However, in practice, it may be prohibitively complicated to enable real-time continuous phase-shifts at the IRS elements due to the hardware limitations. In this context, practical IRS deployments may adopt discrete phase-shifts via phase quantization. To investigate the detrimental impact of quantized phase-shifts, we assume that the IRS controller is only able to select a limited number of discrete quantized phases for the  $n$ th IRS element as

$$\hat{\theta}_n^* = 2\pi\hat{q}/2^b, \quad \forall n, \quad (34)$$

where  $b$  is the number of quantization bits, and  $\hat{q}$  is defined as

$$\hat{q} = \underset{q \in \{0, \pm 1, \dots, \pm 2^{b-1}\}}{\operatorname{argmin}} |\theta_n^* - \pi q/2^{b-1}|, \quad (35)$$

where  $\theta_n^*$  is the optimal phase-shift defined in (5). The error between the unquantized and quantized phase-shift can be defined as

$$\epsilon_n = \theta_n^* - \hat{\theta}_n^*, \quad (36)$$

which tends to be uniformly distributed for a large number of quantization levels, i.e.,  $\epsilon_n \sim \text{Uniform}[-\tau, \tau)$  for  $\tau = \pi/2^b$  [31]. Moreover, this phase error  $\epsilon_n$  becomes uncorrelated with the signal for an increasing number of quantization levels [31]. When IRS elements invoke discrete phase-shifts as per (34), the optimal SNR  $\hat{\gamma}^*$  in (4) can be rewritten as

$$\hat{\gamma}^* = \bar{\gamma} \left| \bar{v} + \sum_{n=1}^N \bar{g}_n \bar{h}_n \eta_n \exp(j\epsilon_n) \right|^2 = \bar{\gamma} \left( (\bar{v} + \tilde{W}_R)^2 + \tilde{W}_I^2 \right), \quad (37)$$

where  $\tilde{W}_R = \sum_{n=1}^N \bar{g}_n \bar{h}_n \eta_n \cos(\epsilon_n)$  and  $\tilde{W}_I = \sum_{n=1}^N \bar{g}_n \bar{h}_n \eta_n \sin(\epsilon_n)$  account for the real and imaginary parts of the reflected signal from the IRS. By invoking Lemma 2, the distribution of  $\tilde{W}_R$  and  $\tilde{W}_I$  can be approximated as lower-tail truncated normal distributions. Specifically, the PDF/CDF of  $W_R$  and  $W_I$  can be deduced from (7) and (8) by replacing  $(\bar{\mu}, \bar{\sigma}^2, \xi)$  with  $(\bar{\mu}_R, \bar{\sigma}_R^2, \xi_R)$  and  $(\bar{\mu}_I, \bar{\sigma}_I^2, \xi_I)$ , respectively. Here,  $\bar{\mu}_R, \bar{\mu}_I, \bar{\sigma}_R^2$ , and  $\bar{\sigma}_I^2$  can be defined as

$$\bar{\mu}_R = \bar{\mu} \sin(\tau)/\tau \quad \text{and} \quad \bar{\mu}_I = 0, \quad (38)$$

$$\bar{\sigma}_R^2 = \left[ \frac{\sin(2\tau)}{4\tau} + \frac{1}{2} \right] \left[ \sum_{n=1}^N \eta_n \kappa_{g_n} \kappa_{h_n} \right] - \bar{\mu}_R^2, \quad \text{and} \quad \bar{\sigma}_I^2 = \left[ \frac{1}{2} - \frac{\sin(2\tau)}{4\tau} \right] \left[ \sum_{n=1}^N \eta_n \kappa_{g_n} \kappa_{h_n} \right]. \quad (39)$$

Moreover,  $\xi_R = 1/\mathcal{Q}(\bar{Z}_R)$ , where  $\bar{Z}_R = -\bar{\mu}_R/\bar{\sigma}_R$  and  $\xi_I = 1/\mathcal{Q}(0) = 2$ . By using (37) and (25), the lower and upper bounds for the achievable rate with quantized phase-shifts are given by<sup>2</sup>

$$\hat{\mathcal{R}}_{lb} = \log_2 \left( 1 + \frac{\bar{\gamma} \left( \kappa_v + 2\mu_{W_R} \Gamma(m_v + 1/2) \sqrt{\kappa_v/m_v} / \Gamma(m_v) + \mu_{W_R}^2 + \sigma_{W_R}^2 + \sigma_{W_I}^2 \right)^3}{\frac{(m_v+1)}{m_v} \kappa_v^2 + 4\bar{\mu}_R \frac{\Gamma(m_v+3/2)}{\Gamma(m_v)} \left[ \frac{\kappa_v}{m_v} \right]^{3/2} + 2(\bar{\mu}_R^2 + \bar{\sigma}_R^2) \sigma_I^2 + \sum_{k=1}^4 I_k} \right), \quad (40a)$$

<sup>2</sup>The derivation follows steps similar to those in Appendix D, and hence, the proofs are omitted for the sake of brevity.

$$\hat{\mathcal{R}}_{ub} = \log_2 \left( 1 + \bar{\gamma} \left( \kappa_v + 2\mu_{W_R} \Gamma(m_v + 1/2) \sqrt{\kappa_v/m_v} / \Gamma(m_v) + \mu_{W_R}^2 + \sigma_{W_R}^2 + \sigma_{W_I}^2 \right) \right), \quad (40b)$$

where  $I_k$  for  $k \in \{1, \dots, 4\}$  are given by

$$I_1 = \frac{\xi_R}{2\sqrt{\pi}} \sum_{i=0}^4 \binom{4}{i} (2\bar{\sigma}_R^2)^{i/2} \mathcal{I} \left( i, -\frac{\bar{\mu}_R}{\sqrt{2\bar{\sigma}_R^2}} \right), \quad I_2 = \frac{\xi_I}{2\sqrt{\pi}} \sum_{i=0}^4 \binom{4}{i} (2\bar{\sigma}_I^2)^{i/2} \mathcal{I}(i, 0), \quad (41a)$$

$$I_3 = \frac{4\Gamma(m_v + 1/2)}{\Gamma(m_v)} \left[ \frac{\kappa_v}{m_v} \right]^{1/2} \left[ \frac{\xi_R}{2\sqrt{\pi}} \sum_{i=0}^3 \binom{3}{i} (2\bar{\sigma}_R^2)^{i/2} \bar{\mu}_R^{3-i} \mathcal{I} \left( i, -\frac{\bar{\mu}_R}{\sqrt{2\bar{\sigma}_R^2}} \right) + \bar{\mu}_R \bar{\sigma}_I^2 \right], \quad (41b)$$

$$I_4 = 2\kappa_v (3(\bar{\sigma}_R^2 + \bar{\mu}_R^2) + \bar{\sigma}_I^2). \quad (41c)$$

In (40a) and (40b),  $\mu_{W_R}$ ,  $\sigma_{W_I}^2$ , and  $\sigma_{W_R}^2$  are given by  $\mu_{W_R} = \bar{\mu}_R + \bar{\sigma}_R \xi_R \phi(\bar{Z}_R)$ ,  $\sigma_{W_I}^2 = \bar{\sigma}^2 (1 - 2/\pi)$ , and  $\sigma_{W_R}^2 = \bar{\sigma}_R^2 (1 + \bar{Z}_R \xi_R \phi(\bar{Z}_R) - (\xi \phi(\bar{Z}_R))^2)$ , where  $\phi(\cdot)$  is defined in Lemma 2.

**Remark 9:** When the IRS consists of a large number of reflective elements and employs quantized phase-shifts, the rate bounds in (40a) and (40b) can be further simplified as follows: For moderately large  $N$ , by following steps similar to those used in Remark 2 and by replacing  $\bar{\mu}_{W_R}$ ,  $\bar{\sigma}_{W_R}^2$ ,  $\bar{\sigma}_{W_I}^2$  and  $\xi_R$  with  $\bar{\mu}_R$ ,  $\bar{\sigma}_R^2$ ,  $\bar{\sigma}_I^2$  and 1, respectively, in (40a) and (40b), the lower and upper bounds for the achievable rate with quantized phase-shifts can be deduced as

$$\hat{\mathcal{R}}_{lb} = \log_2 \left( 1 + \frac{\bar{\gamma} \left( \kappa_v + 2\bar{\mu}_R \Gamma(m_v + 1/2) \sqrt{\kappa_v/m_v} / \Gamma(m_v) + \bar{\mu}_R^2 + \bar{\sigma}_R^2 + \bar{\sigma}_I^2 \right)^3}{\frac{(m_v+1)}{m_v} \kappa_v^2 + 2(\bar{\mu}_R^2 + \bar{\sigma}_R^2) \bar{\sigma}_I^2 + 2\kappa_v (3(\bar{\sigma}_R^2 + \bar{\mu}_R^2) + \bar{\sigma}_I^2) + \sum_{k=1}^4 \bar{I}_k} \right), \quad (42)$$

$$\hat{\mathcal{R}}_{ub} = \log_2 \left( 1 + \bar{\gamma} \left( \kappa_v + 2\bar{\mu}_R \Gamma(m_v + 1/2) \sqrt{\kappa_v/m_v} / \Gamma(m_v) + \bar{\mu}_R^2 + \bar{\sigma}_R^2 + \bar{\sigma}_I^2 \right) \right), \quad (43)$$

where  $\bar{I}_k$  for  $k = \{1, \dots, 4\}$  are given by  $\bar{I}_1 = 4\bar{\mu}_R [\bar{\mu}_R^2 + 3\bar{\sigma}_R^2 + \bar{\sigma}_I^2] \Gamma(m_v + 1/2) (\kappa_v/m_v)^{1/2} / \Gamma(m_v)$ ,  $\bar{I}_2 = 4\bar{\mu}_R \Gamma(m_v + 3/2) (\kappa_v/m_v)^{3/2} / \Gamma(m_v)$ ,  $\bar{I}_3 = 3\bar{\sigma}_I^2$ , and  $\bar{I}_4 = \bar{\mu}_R^4 + 6\bar{\mu}_R^2 \bar{\sigma}_R^2 + 3\bar{\sigma}_R^2$ .

## V. THE IMPACT OF SEVERITY OF FADING AND THE UNDERLYING TECHNICAL INSIGHTS

In this section, we discuss the impact of different degrees of severity of channel fading, and thereby, we draw the underlying technical insights. We deduce some useful design insights from the derived performance metrics in Section III.

### A. Performance insights in different fading environments

1) *All channels undergo Rayleigh fading:* When the system operates over Rayleigh fading, the direct and reflected channel models can be deduced by setting the Nakagami- $m$  fading parameters as  $m_v = m_g = m_h = 1$ . Specifically, Rayleigh fading models rich-scattering and can be used to capture more severe fading environments than Nakagami- $m$  model for  $m > 1$  case. In this context, the outage probability, average SER, and achievable rate bounds for Rayleigh fading can be deduced by letting  $m_v = m_g = m_h = 1$  in (19), (31), (26), and (27), respectively. Moreover, the achievable diversity order for the Rayleigh fading case is  $G_d = 1 + N$ .

2) *Direct channel undergoes severe fading:* In a practical deployment, the IRS may be placed at specific places such as on outer-walls of a high-rise building and windows in which the reflected channel may be accessible to a receiver. However, it is not always guaranteed the availability of a less severe direct channel between  $S$  and  $D$ . Thus, this direct channel is more likely to undergo much severe fading. This propagation condition can be modeled by letting  $m_v = 1/2$  in (1), which captures the most severe type of fading case [24]. This choice statistically models the direct channel to be a single-sided Gaussian fading. The outage probability for this asymmetric fading case can be derived as

$$P_{out}^{(SG)} \approx 1 - \frac{\lambda}{2} \bar{\sigma}^2 \left[ \Gamma \left( \frac{1}{2}, ((\sqrt{\gamma_{th}/\bar{\gamma}} - \bar{\mu})/2\sqrt{a}\bar{\sigma}^2)^2 \right) e^{-\Delta((\sqrt{\gamma_{th}/\bar{\gamma}} - \bar{\mu})/2\sqrt{a}\bar{\sigma}^2)^2} - (\Delta + 1)^{-1/2} \Gamma \left( 1/2, (\Delta + 1) ((\sqrt{\gamma_{th}/\bar{\gamma}} - \bar{\mu})/2\sqrt{a}\bar{\sigma}^2)^2 \right) \right]. \quad (44)$$

In deriving (44), we assume that the large-scale fading parameters and the reflection coefficient are the same for all reflective elements at the IRS; i.e.,  $\kappa_{a_n} = \kappa_a$  for  $a \in \{g, h\}$  and  $\eta_n = \eta$ ,  $\forall n$  for the sake of mathematical tractability. The corresponding achievable rate and average SER bounds can be readily obtained by letting  $m_v = 1/2$  in (26), (27), and (31), respectively.

3) *Direct channel is unavailable:* The direct channel between  $S$  and  $D$  may be fully unserviceable due to severe blockage effects. In this case, the end-to-end communication takes place solely via the IRS reflected channel. Then, the outage probability, average SER, and rate bounds can be derived by letting  $\kappa_v \rightarrow 0$  (equivalently,  $\zeta_v \rightarrow 0$ ) in (19), (31), (26), and (27).

### B. Impact of spatially-correlated fading

Once a large number of reflective elements is embedded with an IRS with a fixed area, the incident and reflected channels must be modeled to capture spatially correlated fading. To this end, the correlation effects of  $S$ -to-IRS and IRS-to- $D$  channels are modeled by considering IRS as a uniformly distributed 2D square array of reflective elements. Without-loss of generality, it is assumed that IRS is placed in the far-field of  $S$  and  $D$ . The angles-of-arrival (AoAs) and angles-of-departure (AoDs) at the IRS are assumed to be randomly distributed in azimuth and elevation planes as  $\Omega_i \sim \mathcal{CN}(\omega_i, \nu_i^2)$  and  $\Psi_i \sim \mathcal{CN}(\psi_i, \delta_i^2)$ , respectively, where  $i = A$  and  $i = D$  are used to denote AoA and AoD. Then, the spatial correlation at the IRS can be modeled as  $\mathbf{R}_i = \mathbf{R}_{i,az} \otimes \mathbf{R}_{i,el}$ , where  $\mathbf{R}_i$  for  $i \in \{A, D\}$  are the spatial correlation matrices at the IRS for incident and reflected signals. Here,  $\mathbf{R}_{i,el}$  and  $\mathbf{R}_{i,az}$  can be modeled as [32]

$$[\mathbf{R}_{i,el}]_{x,y} = e^{j(2\pi d_{el}(y-x) \cos \psi_i)} e^{-\left(\frac{1}{2}(\delta_i 2\pi d_{el})^2 (y-x)^2 \sin^2 \psi_i\right)}, \quad (45)$$

$$[\mathbf{R}_{i,az}]_{r,t} = a_1^{-1/2} e^{-\left(\frac{a_2 \cos^2 \omega_i}{2a_3} + \frac{(a_1 \nu_i)^2 \sin^2 \omega_i}{2a_3}\right)} e^{j \frac{a_1 \cos \omega_i}{a_3}}, \quad (46)$$

where  $a_1 = (2\pi d_{az})(t-r) \sin \psi_i$ ,  $a_2 = \delta_i(2\pi d_{az})(t-r) \cos \psi_i$ , and  $a_3 = a_2^2 \nu_i^2 \sin^2 \omega_i + 1$ . In (45) and (46),  $d_{az}$  and  $d_{el}$  are the distances between the adjacent elements (measured in multiples of wavelengths) in elevation and azimuth planes, respectively. Under spatially correlated fading, the  $S$ -to-IRS and IRS-to- $D$  channels can be modeled as

$$\tilde{\mathbf{g}}^T = \mathbf{g}^T \mathbf{R}_D^{1/2} \quad \text{and} \quad \tilde{\mathbf{h}} = \mathbf{R}_A^{1/2} \mathbf{h}, \quad (47)$$

where  $\mathbf{g}^T = [g_1 \cdots, g_n \cdots, g_N]$  and  $\mathbf{h} = [h_1 \cdots, h_n \cdots, h_N]^T$ . Here  $h_n$  and  $g_n$  are defined in Section II-A and the resulting SNR can be written as

$$\tilde{\gamma} = \bar{\gamma} \left| \bar{v} \exp(j\phi_v) + \mathbf{g}^T \mathbf{R}_D^{1/2} \mathbf{\Theta} \mathbf{R}_A^{1/2} \mathbf{h} \right|^2, \quad (48)$$

where  $\mathbf{\Theta}$  is an  $N \times N$  diagonal matrix whose  $n$ th diagonal element is given by  $[\mathbf{\Theta}]_{n,n} = \eta_n e^{j\theta_n}$ , which denotes the reflection coefficient of the  $n$ th IRS element.

We observe that in the presence of spatially correlated fading, the IRS phase-shifts can be optimized by also considering the phases introduced by correlation matrices in (45) and (46) in addition to the phases of the independently faded channels  $\tilde{\mathbf{g}}^T$  and  $\tilde{\mathbf{h}}$ . To this end, the phase-shift of each IR element, which maximizes the SNR, can be computed as

$$\theta_n^* = \phi_v - (\tilde{\phi}_{h_n} + \tilde{\phi}_{g_n}), \quad \text{for } 1 \leq n \leq N, \quad (49)$$

where  $\tilde{\phi}_{g_n}$  and  $\tilde{\phi}_{h_n}$  are the phases of  $[\tilde{\mathbf{g}}^T]_{1,n}$  and  $[\tilde{\mathbf{h}}]_{n,1}$ , respectively, and they include the cumulative phases  $(\mathbf{g}^T, \mathbf{h})$  and  $(\mathbf{R}_D^{1/2}, \mathbf{R}_A^{1/2})$  in (47). Then, the optimal SNR is given by

$$\tilde{\gamma}^* = \bar{\gamma} \left| \bar{v} + \hat{\mathbf{g}}^T \boldsymbol{\eta} \hat{\mathbf{h}} \right|^2. \quad (50)$$

where  $\boldsymbol{\eta}$  is  $N \times N$  diagonal matrix with  $\eta_n$  as the  $n$ th diagonal element. Moreover,  $\hat{\mathbf{g}}^T$  and  $\hat{\mathbf{h}}$  denote the vectors with the moduli of the elements of  $\mathbf{g}^T$  and  $\mathbf{h}$ , respectively.

## VI. NUMERICAL RESULTS

In this section, our numerical results are presented to validate our analysis, investigate performance gains, and draw useful design insights. In our simulations, the path-loss is modeled as  $\zeta_a [\text{dB}] = \zeta_0 + 10v \log(d)$ , where  $\zeta_a \in \{\zeta_v, \zeta_g, \zeta_h\}$ ,  $\zeta_0 = 42 \text{ dB}$  is a reference path-loss,  $v = 3.5$  is the path-loss exponent, and  $d$  is the distance in meters. Unless otherwise specified, the amplitude attenuation coefficient is set to  $\eta_n = 0.9, \forall n \in \{1, \cdots, N\}$ .

In Fig. 4a, we plot the average achievable rate as a function of average transmit SNR for different numbers of reflective elements at the IRS as  $N = [8, 16, 32, 64, 128]$ . The analytical curves for the lower and upper rate bounds are plotted via (26) and (27), respectively. The exact/optimal achievable rate is also plotted via Monte-Carlo simulations for comparison purposes. We observed from Fig. 4a that our rate bounds are tight even for a small number of IRS elements



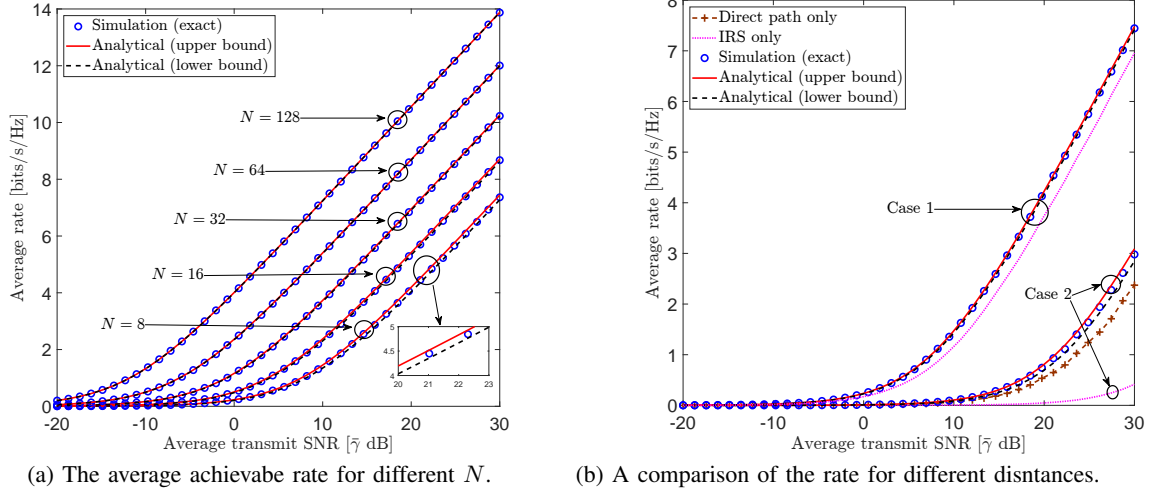


Fig. 4. The average rate versus average transmit SNR for  $(m_v, m_g, m_h) = (2, 3, 4)$  and  $d_{SD} = 100$  m. In Fig. 4a,  $d_{SI} = d_{DI} = 60$  m. In Fig. 4b, the distances for Case-1 and Case-2 are set to  $d_{SI} = d_{DI} = 60$  m, and  $d_{SI} = d_{DI} = 140$  m.

such as  $N = 8$ , and they converge to the exact simulation with increasing  $N$  (see  $N = 128$  case in Fig. 4a). Moreover, higher the number of reflective elements at IRS, higher the achievable rate. For example, at an average SNR of 20 dB, the average rate can be increased by 1.9 bits/s/Hz and 3.1 bits/s/Hz, respectively, when the number of IRS elements is doubled and quadrupled in comparison to  $N = 16$  case.

Fig. 4b provides a comparison of the average achievable rate for the IRS-assisted system with respect to a baseline direct transmission between  $S$  and  $D$ . Moreover, the average rate for the IRS only case (without the direct channel) is also plotted. To highlight the performance gain of IRS, two system configurations in which IRS is placed such that  $d_{SD} \approx d_{SI} + d_{ID}$  (Case-1) and  $d_{SD} \ll d_{SI} + d_{ID}$  (Case-2) are considered. Fig. 4b clearly shows that the cases, where the direct transmission is aided by IRS, outperforms all other cases throughout the useful SNR regime regardless of the distance to the IRS. When the direct channel is unserviceable, the IRS-aided system can provide significant rate gains provided that the IRS is placed nearer to  $S$  and  $D$  as in Case-1. However, when the IRS is placed further away from  $S$  and  $D$ , the distance-dependent path-loss effects hinder the rate performance gains of the IRS. Specifically, at an average SNR of 25 dB, Case-1 provides a rate gain of 4.492 bits/s/Hz over the direct transmission. However, in Case-2, a rate gain of 0.486 bits/s/Hz is achieved over the direct transmission at the same average SNR. Thus, the placements of IRS with respect to  $S$  and  $D$  has a significant impact on the achievable rate gains. This is primarily due to the fact that beamforming gains attainable via passive reflections at the IRS may not be able to overcome the larger path-losses when the IRS is placed far away from  $S$  and  $D$ .

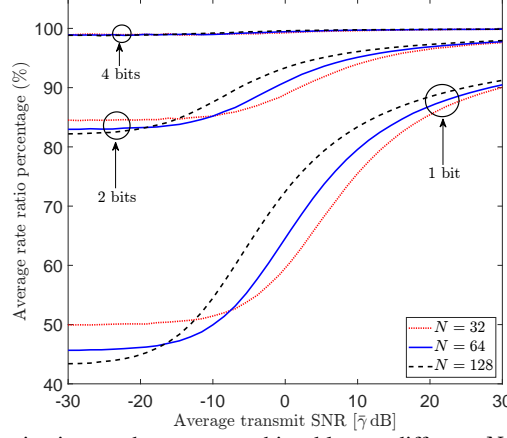


Fig. 5. The impact of phase-shift quantization on the average achievable rate different  $N$  values. The average rate percentage =  $\frac{\hat{\mathcal{R}}}{\mathcal{R}} \times 100\%$ , where  $\hat{\mathcal{R}}$  and  $\mathcal{R}$  are the average achievable rates with and without phase-shift quantization errors, respectively. Here,  $(m_v, m_g, m_h) = (2, 3, 4)$ ,  $d_{SD} = 100$  m, and  $d_{SI} = d_{DI} = 60$  m.

Fig. 5 is used to investigate the impact of the number of quantization bits ( $b$ ) used for IRS phase-shift controlling, where the phase quantization error is randomly generated within  $[-\pi/2^b, \pi/2^b]$ . The underlying detrimental impact is quantified by computing the average rate percentage, which is defined as the percentage of the rate gain that can be achieved by employing quantized phase-shifts at the IRS elements with respect to the benchmark system, where continuous phase-shifts are allowed with no phase errors. In this context, the average rate percentage can be defined as follows: average rate percentage =  $\frac{\hat{\mathcal{R}}}{\mathcal{R}} \times 100\%$ , where  $\hat{\mathcal{R}}$  and  $\mathcal{R}$  are the average achievable rates with and without phase-shift quantization errors, respectively. According to Fig. 5, when  $b$  is increased, the effect of phase errors becomes negligible. In particular, with 4 bit quantization at all IRS elements, more than 98% of the average rate can be recovered with respect to the continuous phase-shifts. Moreover, the average rate percentage improves with the transmit SNR. For example, more than 80%, 95%, and almost 100% of the rate gains can be recovered with 1, 2 and 4 bit quantization, respectively, when the transmit SNR is maintained beyond 20 dB ( $\bar{\gamma} \geq 20$  dB). Moreover, in Fig. 5, the average rate percentage curves are plotted for  $N = [32, 64, 128]$ . While increasing number of IRS elements is beneficial in moderate-to-large SNR regime, it detrimentally affects the rate performance in low SNR regime. This is primarily due to the adverse effects of quantization errors becoming increasingly dominant with increasing  $N$  in the low SNR regime.

In Fig. 6, the outage probability of the IRS-aided system is investigated. To this end, our outage probability (19) and the asymptotic outage in high SNR regime (21) are plotted as a function of the average transmit SNR for  $N = [8, 16, 32]$ . Moreover, Monte-Carlo simulations for the outage probability are presented. Tightness of our outage probability analysis improves with increasing

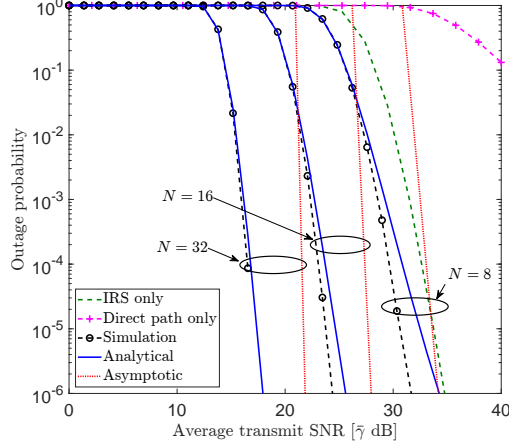


Fig. 6. The outage probability versus the average transmit SNR for different numbers of IRS elements with  $\gamma_{th} = 10$  dB,  $(m_v, m_g, m_h) = (2, 2, 3)$ ,  $d_{SD} = 100$  m, and  $d_{SI} = d_{DI} = 60$  m.

$N$ . The negative gradient of the asymptotic outage curves in Fig. 6 can be computed to obtain the achievable diversity order. For instance, in the case of  $N = 16$ , the negative gradient of the asymptotic outage curve is  $-(\log_{10}(0.9512) - \log_{10}(0.00001944)) \times 10 / (26.21 - 27.59) \approx 34$ , which exactly agrees with our diversity order analysis in (22);  $G_d = m_v + \min(m_g, m_h)N = 2 + \min(2, 3) \times 16 = 34$ . Moreover, the achievable diversity order can be boosted 266.6% by increasing the number of reflected elements from  $N = 8$  to  $N = 32$ . Thus, this observation verifies our asymptotic performance analysis that the diversity order can be drastically increased by increasing  $N$  of the IRS. It is noteworthy to mention that this diversity gain is achieved by merely employing passive IRS reflective elements without using costly active RF chains. Moreover, in Fig. 6, the outage probability curves of the direct channel (without the IRS) and sole IRS-aided ( $N = 8$ ) system (without the direct channel) are plotted for comparison purposes. These outage curves clearly depicts that the passive reflections of the IRS can indeed boost the outage performance. For instance, the sole direct transmission cannot achieve an outage of  $10^{-2}$  even with an average SNR of 40 dB. However, when an IRS with  $N = 8$  is deployed without the direct channel, an average SNR of 30 dB is sufficient to achieve the same outage probability.

In Fig. 7a, the average bit error rate (BER) of BPSK and the asymptotic BER analysis in high SNR regime are plotted and are compared with the direct transmission between  $S$  and  $D$ . In Cases-1, 2 and 3, the IRS is placed, respectively, at a closer location to  $S$  and  $D$  such that  $d_{SD} \approx d_{SI} + d_{ID}$  (Case-1), at a moderate distance according to  $d_{SD} < d_{SI} + d_{ID}$  (Case-2), and at a far-away location such that  $d_{SD} \ll d_{SI} + d_{ID}$  (Case-3). The transmission distance of the direct channel is  $d_{SD}$  at 100 m. Since both direct and reflected signals are co-phased, the IRS-assisted system outperforms the direct transmission in all three cases. For example, to

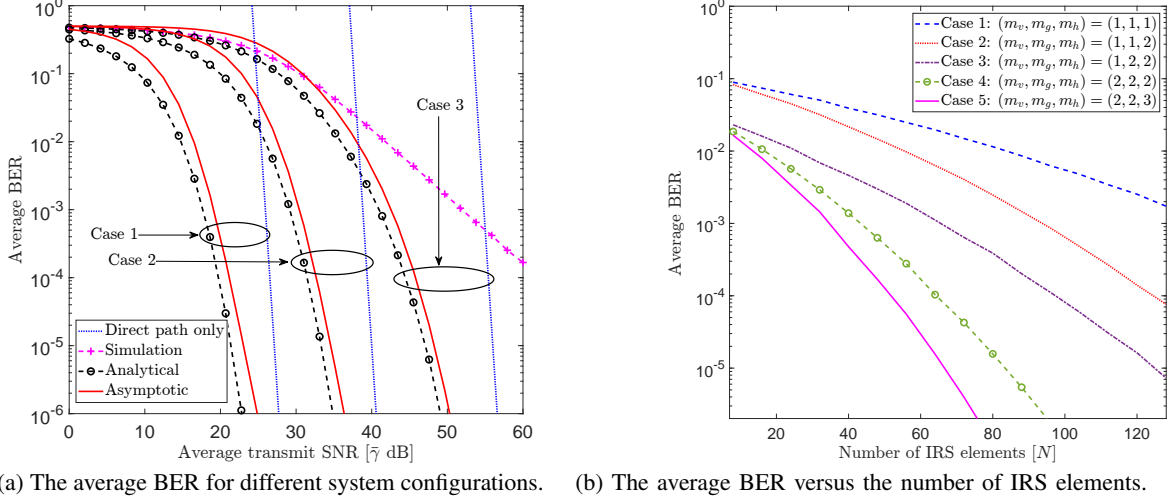


Fig. 7. An average BER comparison for BPSK with  $\alpha = 1$ ,  $\beta = 2$  in (31). For all cases,  $d_{SD} = 100$  m. In 7a,  $(m_v, m_g, m_h) = (1, 1, 2)$ ,  $N = 16$ , the distances for Case-1 to Case-3 are set to  $d_{SI} = d_{DI} = 51$  m,  $d_{SI} = d_{DI} = 80$  m, and  $d_{SI} = d_{DI} = 140$  m, respectively. In Fig. 7b,  $d_{SI} = d_{DI} = 140$  m and  $\bar{\gamma} = 30$  dB.

obtain an average BER of  $10^{-2}$ , the direct transmission needs an average SNR of 41.86 dB. However, when an IRS is placed at a far-away location (Case-3), this SNR requirement can be reduced by 4 dB. Furthermore, when compared with the direct transmission, to achieve the same average BER of  $10^{-2}$ , the SNR requirement can be significantly lowered by around 10.5 dB and 21.5 dB when the IRS is placed at moderate (Case-2) and closer (Case-1) distances, respectively. Thus, these observations reveal that the average BER performance of IRS-assisted systems heavily depends on the placement of the IRS with respect to  $S$  and  $D$ . This is because, IRS only facilitates the end-to-end direct transmission by virtue of passive reflections, and if the transmission distances of the reflected channels are high, then the underlying large-scale fading losses cannot be compensated by passive beamforming gains provided by phase-shift control at the IRS. The negative gradient of the asymptotic BER curves in Fig. 7a is  $-(\log_{10}(0.01) - \log_{10}(0.0001))10/(38.27 - 39.47) \approx 17$ . This observation verifies our high SNR BER analysis in (22) such that  $G_d = m_v + \min(m_g, m_h)N = 1 + \min(1, 2) \times 16 = 17$ . It is also worth noting that the diversity orders for all three cases are the same because three average BER curves are plotted by varying the distances and keeping  $N$ ,  $m_v$ ,  $m_g$ , and  $m_h$  fixed.

In Fig. 7b, the effects of number of reflective elements ( $N$ ) and asymmetric channel fading conditions are investigated by plotting the average BER of BPSK as a function of  $N$  by varying the severity of fading parameters  $(m_v, m_g, m_h)$ . Fig. 7b reveals that the average BER performance improves with higher  $N$ . For example, the numbers of IRS elements required to achieve an average BER of  $10^{-2}$  at  $\bar{\gamma} = 30$  dB are 84, 56, 26, 16, and 9 for Case-1 to Case-5, respectively. Moreover, the average BER reduces with higher  $(m_v, m_g, m_h)$ . This is because

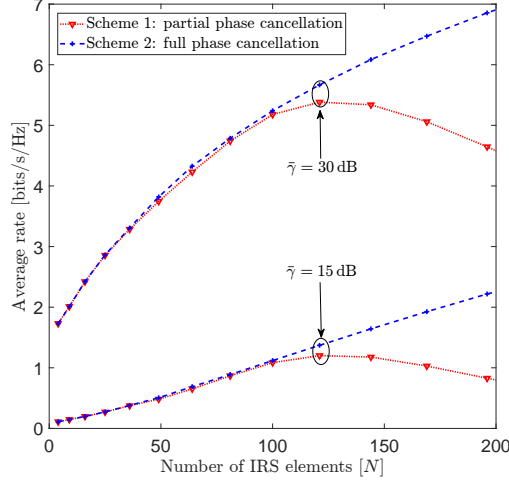


Fig. 8. Impact of spatial correlation over Rician fading. The Rician factors for  $v$ ,  $g$ , and  $h$  channels are given by  $K_v = 2$ ,  $K_g = 3$ , and  $K_h = 4$ , respectively. The area of IRS is  $1 \times 1 \text{ m}^2$ ,  $d_{SD} = 100 \text{ m}$ ,  $d_{SI} = d_{DI} = 80 \text{ m}$ , and  $\lambda = 0.1 \text{ m}$ .

higher  $(m_v, m_g, m_h)$ , less severe the fading conditions as per Nakagami- $m$  fading model. Thus, this observation indicates that by placing the IRS such that the reflected channels undergo milder fading conditions can improve the performance of IRS-aided systems. This insight is in-line with the original idea of coating building walls, windows and hallways with IRS to minimize channel blockages/obstructions and thereby facilitate reliable wireless access.

In Fig. 8, the impact of spatially correlated fading is investigated by plotting the average achievable rate as a function of the number of reflective elements ( $N$ ) when the surface area of IRS is restricted to  $1 \times 1 \text{ m}^2$ . The co-phasing of received signals at  $D$  is achieved by via (49) by considering the correlation matrices at the IRS, and the corresponding rate curves are denoted by Scheme-2. To reveal the detrimental impact of spatial correlation, the rate curves without considering the additional phases introduced by correlation are also plotted and the underlying curves are denoted by Scheme-1. The achievable rates of the Scheme-2 clearly outperform Scheme-1 when  $N$  grows large. This is because, the impact of correlation becomes more severe when a large number of reflective elements are embedded in a given surface area, and the Scheme-2 is designed to cancel the correlation effects, whereas in Scheme-1, the spatial correlation matrices at the IRS are not considered in designing IRS phase-shifts. Thus, in Scheme-2, the received signals via the direct and reflected channels can be perfectly co-phased, while the same is not possible in Scheme-1. This observation reveals that the deleterious impact of spatial correlation can be fully mitigated by intelligently controlling the IRS phase-shifts when the spatial correlation matrices are known.

## VII. CONCLUSION

In this paper, the performance of IRS-assisted wireless communication system over Nakagami- $m$  fading has been investigated. The optimal IRS phase-shifts to maximize the received SNR have been quantified, and thereby, the probability distributions of this optimal SNR have been approximated by using the CLT. The fundamental performance bounds, including tight approximations to the outage probability, average SER, and achievable rate bounds have been derived in closed-form. The accuracy of these performance metrics has been validated via numerical results, and it has been revealed that the tightness of our approximations/bounds improves when the number of IRS reflective elements grows large. The achievable diversity order has been quantified by deriving a single-polynomial high SNR approximation of the CDF of the optimal SNR. Thereby, we reveal that the diversity order can be increased linearly with the number of passive IRS reflective elements, and this diversity gain is achieved without deploying additional RF chains in the system. It has been shown that our lower/upper rate bounds become asymptotically exact in large  $N$  regime, and the transmit power can be scaled inversely proportional to  $N^2$ . The deleterious effects of quantized IRS phase-shifts have been investigated by deriving the achievable rate bounds, and consequently, it has been revealed that the rate losses due to phase-shift quantization errors can be circumvented in the large IRS reflective element regime. Further, the deleterious impact of spatially correlated fading has been investigated. By virtue of our analysis and numerical results, we show that the performance of wireless communication systems can be significantly improved by coating physical objects in the propagation channel with the IRS having passive reflective elements and intelligently controlling their phase-shifts.

### APPENDIX A PROOF FOR LEMMA 2

The RVs  $\bar{h}_n$  and  $\bar{g}_n$  for  $n \in \{1, \dots, N\}$  in (4) are independently distributed. Next, we define  $\tilde{W}_n = \eta_n \bar{g}_n \bar{h}_n$  such that it generates a sequence of independent RVs  $\{\tilde{W}_1, \dots, \tilde{W}_n, \dots, \tilde{W}_N\}$ ; each with mean  $\mu_{\tilde{W}_n}$  and variance  $\sigma_{\tilde{W}_n}^2$ . Specifically,  $\mu_{\tilde{W}_n}$  and  $\sigma_{\tilde{W}_n}^2$  can be derived as

$$\mu_{\tilde{W}_n} = \mathbb{E}[\eta_n \bar{g}_n \bar{h}_n] \stackrel{(a)}{=} \eta_n \mathbb{E}[\bar{g}_n] \mathbb{E}[\bar{h}_n] = \eta_n \sqrt{\frac{\kappa_{g_n} \kappa_{h_n}}{m_g m_h}} T(m_g, m_h, 1/2), \quad (51)$$

$$\sigma_{\tilde{W}_n}^2 = \mathbb{E}[(\eta_n \bar{g}_n \bar{h}_n)^2] - \mu_{\tilde{W}_n}^2 \stackrel{(b)}{=} \eta_n^2 \mathbb{E}[\bar{g}_n^2] \mathbb{E}[\bar{h}_n^2] - \mu_{\tilde{W}_n}^2 \stackrel{(c)}{=} \eta_n^2 \kappa_{g_n} \kappa_{h_n} - \mu_{\tilde{W}_n}^2, \quad (52)$$

where  $T(a, b, i)$  is defined in Lemma 2. In steps (a) and (b), the fact that  $\bar{g}_n$  and  $\bar{h}_n$  are independent RVs is invoked. The square of a Nakagami- $m$  distributed RV follows a Gamma distribution, i.e.,  $\bar{a}_n^2 \sim \text{Gamma}(m_a, \kappa_{a_n}/m_a)$ , and hence, in the step (c), we invoke  $\mathbb{E}[\bar{a}_n^2] = \kappa_{a_n}$

for  $\bar{a} \in \{\bar{g}, \bar{h}\}$  [33]. The distribution of  $\tilde{W} = \sum_{n=1}^N \tilde{W}_n$  approaches to a lower-tail truncated normal distribution if it satisfies the following sufficient conditions [24]; (i)  $\sum_{n=1}^N \sigma_{\tilde{W}_n}^2 \xrightarrow{N \rightarrow \infty} \infty$ , and (ii) there exists a number  $\alpha > 2$  and a finite constant  $M$  such that  $\mathbb{E}[\tilde{W}_n^\alpha] < M < \infty$  for all  $n \in \{1, \dots, N\}$ . It can be shown that  $\tilde{W}$  satisfies the first condition because of the fact that

$$\lim_{N \rightarrow \infty} \sum_{n=1}^N \sigma_{\tilde{W}_n}^2 = \left(1 - \frac{T^2(m_g, m_h, 1/2)}{m_g m_h}\right) \left[ \lim_{N \rightarrow \infty} \sum_{n=1}^N \eta_n^2 \kappa_{g_n} \kappa_{h_n} \right] \xrightarrow{(d)} \infty, \quad (53)$$

where the step (d) is possible since  $\eta_n^2 \kappa_{g_n} \kappa_{h_n} > 0, \forall n$ , and as  $N$  grows large,  $\sum_{n=1}^N \eta_n^2 \kappa_{g_n} \kappa_{h_n}$  approaches infinity. Next, via the steps similar to (52),  $\mathbb{E}[\tilde{W}_n^\alpha]$  can be computed as

$$\mathbb{E}[\tilde{W}_n^\alpha] = \eta_n^\alpha \mathbb{E}[\bar{g}_n^\alpha] \mathbb{E}[\bar{h}_n^\alpha] = T(m_g, m_h, \alpha/2) \left[ \frac{\eta_n^2}{\kappa_{g_n} \kappa_{h_n}} \right]^{\alpha/2}. \quad (54)$$

Thus, there exists a finite  $M$  such that  $\mathbb{E}[\tilde{W}_n^\alpha] < M < \infty, \forall n$  for some  $\alpha$ , where  $T(m_g, m_h, \alpha/2) \times [\eta_n^2 / \kappa_{g_n} \kappa_{h_n}]^{\alpha/2} < M$ . This completes the proof that  $W$  satisfies sufficient conditions, and thus,  $F_W(w)$  can be approximated by a lower-tail truncated normal distribution as stated in Lemma 2 with  $\mu_W$  and  $\sigma_W^2$ , which are given in (10).

## APPENDIX B DERIVATION OF THE CDF OF $\gamma$ IN (14)

To begin with, by defining the received signal envelope as  $R = \bar{v} + W$ , we rewrite (4) as  $\gamma = \bar{\gamma} R^2$ . Since,  $\bar{v}$  and  $W$  are independent RVs, the PDF of  $R$  can be derived as [24]

$$\begin{aligned} f_R(r) &= \int_0^\infty f_{\bar{v}}(u) f_W(r-u) du = 2a^{m_v} \lambda e^{-\frac{(r-\bar{\mu})^2}{2\bar{\sigma}^2}} \int_0^\infty u^{\tilde{m}_v} e^{-au^2 + ub(r)} du \\ &= 2a^{m_v} \lambda e^{-\frac{(r-\bar{\mu})^2}{2\bar{\sigma}^2}} e^{\frac{b^2(r)}{4a}} \underbrace{\int_0^\infty u^{\tilde{m}_v} e^{-a(u - \frac{b(r)}{2a})^2} du}_{I_R(r)}, \end{aligned} \quad (55)$$

where  $\tilde{m}_v = 2m_v - 1$ , and  $b(r)$  denotes a function of  $r$  defined by  $b(r) = (r - \bar{\mu})/\bar{\sigma}^2$ . In (55),  $a$  and  $\lambda$  are defined in (15). Substituting  $t = \sqrt{a}(u - b(r)/2a)$ ,  $I_R(r)$  in (55) can be rewritten as

$$I_R(r) = \frac{1}{a^{m_v}} \int_{-\tilde{b}(r)}^\infty \left(t + \tilde{b}(r)\right)^{\tilde{m}_v} e^{-t^2} dt = \frac{1}{a^{m_v}} \sum_{k=0}^{\tilde{m}_v} \binom{\tilde{m}_v}{k} \left(\tilde{b}(r)\right)^{\tilde{m}_v-k} \mathcal{I}(k, -\tilde{b}(r)), \quad (56)$$

where  $\tilde{b}(r) = (r - \bar{\mu})/(2\bar{\sigma}^2\sqrt{a})$  and  $\mathcal{I}(q, x) = \int_x^\infty t^q e^{-t^2} dt$ . For  $x \geq 0$ ,  $\mathcal{I}(q, x) = \Gamma((q+1)/2, x^2)/2$ , and when  $x < 0$ ,  $\mathcal{I}(q, x)$  can be written as  $\mathcal{I}(q, x) = \int_{-\infty}^\infty t^q e^{-t^2} dt - \int_{-\infty}^{-x} t^q e^{-t^2} dt$ , which can be evaluated in closed-form as (17). By substituting  $\mathcal{I}(k, -\tilde{b}(r))$  into (56),  $I_R(r)$  can be evaluated, and then, by using the resulting expression,  $f_R(r)$  in (55) can be derived as

$$f_R(r) = \begin{cases} \lambda e^{-\Delta \left(\frac{r-\bar{\mu}}{2\sqrt{a}\bar{\sigma}^2}\right)^2} \sum_{k=0}^{\tilde{m}_v} \binom{\tilde{m}_v}{k} \left(\frac{r-\bar{\mu}}{2\bar{\sigma}^2\sqrt{a}}\right)^{\tilde{m}_v-k} \Gamma\left(\frac{k+1}{2}, \left(\frac{r-\bar{\mu}}{2\bar{\sigma}^2\sqrt{a}}\right)^2\right) & r \leq \bar{\mu}, \\ \lambda e^{-\Delta \left(\frac{r-\bar{\mu}}{2\sqrt{a}\bar{\sigma}^2}\right)^2} \sum_{k=0}^{\tilde{m}_v} \binom{\tilde{m}_v}{k} \left(\frac{r-\bar{\mu}}{2\bar{\sigma}^2\sqrt{a}}\right)^{\tilde{m}_v-k} \left[ \Gamma\left(\frac{k+1}{2}\right) + (-1)^k \gamma\left(\frac{k+1}{2}, \left(\frac{r-\bar{\mu}}{2\bar{\sigma}^2\sqrt{a}}\right)^2\right) \right] & r > \bar{\mu}, \end{cases} \quad (57)$$

and  $f_R(r) = 0$  otherwise.

Next, the derivation of the CDF of  $R$  is outlined. For  $0 < r \leq \bar{\mu}$ , the CDF of  $R$  can be written as  $F_R(r) = \int_0^r f_R(y)dy$ . By substituting (57),  $F_R(r)$  can be written as

$$F_R(r) = \sum_{k=0}^{\tilde{m}_v} 2\lambda\sqrt{a}\bar{\sigma}^2 \binom{\tilde{m}_v}{k} J_1, \text{ for } 0 < r \leq \bar{\mu}. \quad (58)$$

In (58),  $J_1$  is given by

$$J_1 = \int_0^r \frac{(\tilde{b}(y))^{\tilde{m}_v-k} e^{-\Delta(\tilde{b}(y))^2}}{2\sqrt{a}\bar{\sigma}^2} \Gamma\left(\frac{k+1}{2}, (\tilde{b}(y))^2\right) dy. \quad (59)$$

By substituting  $t = -\tilde{b}(y)$ ,  $J_1$  can be rewritten as

$$J_1 = (-1)^{\tilde{m}_v-k} \left[ \mathcal{J}(k, -\tilde{b}(0)) - \mathcal{J}(k, -\tilde{b}(r)) \right], \quad (60)$$

where  $\mathcal{J}(k, \delta)$  is given by

$$\mathcal{J}(k, z) = \int_z^\infty t^{\tilde{m}_v-k} e^{-\Delta t^2} \Gamma\left(\frac{k+1}{2}, t^2\right) dt. \quad (61)$$

Next, (61) can be evaluated separately for odd and even values of  $k$  as follows: When  $k$  is odd,  $\delta_o = (k+1)/2$  becomes an integer, and we expand  $\Gamma((k+1)/2, t^2)$  in (61) as  $\Gamma((k+1)/2, t^2) = (\delta_o - 1)! e^{-t^2} \sum_{i=0}^{\delta_o-1} t^{2i}/i!$  [23, 8.352.7]. For odd values of  $k$ ,  $\mathcal{J}(k, z)$  can be rewritten as

$$\mathcal{J}_o(k, z) = (\delta_o - 1)! \sum_{i=0}^{\delta_o-1} \frac{1}{i!} \int_z^\infty t^{\tilde{m}_v-k+2i} e^{-(\Delta+1)t^2} dt. \quad (62)$$

By using [23, 2.33.10],  $\mathcal{J}_o(k, z)$  can be evaluated in closed-form as (18a). For even values of  $k$ ,  $\delta_e = m_v - k/2$  becomes an integer, and we have [23, 2.33.11]

$$\int t^{\tilde{m}_v-k} e^{-\Delta t^2} dt = \frac{(\delta_e - 1)!}{2} \sum_{j=0}^{\delta_e-1} -\frac{e^{-\Delta t^2} t^{2j}}{j! \Delta^{\delta_e-1}}. \quad (63)$$

Thus,  $\mathcal{J}(k, z)$  can be evaluated by using integration-by-parts as follows:

$$\mathcal{J}_e(k, z) = \frac{(\delta_e - 1)!}{2} \sum_{j=0}^{\delta_e-1} \frac{e^{-\Delta z^2} z^{2j}}{j! \Delta^{\delta_e-1}} \Gamma\left(\frac{k+1}{2}, z^2\right) - (\delta_e - 1)! \sum_{j=0}^{\delta_e-1} \frac{\Delta^{\delta_e-1}}{j!} \int_z^\infty t^{k+2j} e^{-(\Delta+1)t^2} dt. \quad (64)$$

By invoking [23, 2.33.10],  $\mathcal{J}_e(k, z)$  can be evaluated in closed-form as (18b). Depending on the value of  $k$ , by substituting (18a) or (18b) into (60), the desired expression for  $J_1$  can be derived next. For  $r > \bar{\mu}$ ,  $F_R(r) = 1 - \int_r^\infty f_R(y)dy$ . By substituting (57),  $F_R(r)$  can be written as

$$F_R(r) = 1 - \sum_{k=0}^{\tilde{m}_v} 2\lambda\sqrt{a}\bar{\sigma}^2 \binom{\tilde{m}_v}{k} (I_2 - J_2) \text{ for } r > \bar{\mu}, \quad (65)$$



where  $I_2$  and  $J_2$  can be defined as

$$I_2 = \frac{[(-1)^k + 1]\Gamma\left(\frac{k+1}{2}\right)}{2\sqrt{a}\bar{\sigma}^2} \int_r^\infty \left(\tilde{b}(y)\right)^{\tilde{m}_v-k} e^{-\Delta(\tilde{b}(y))^2} dy, \quad (66)$$

$$J_2 = (-1)^k \int_r^\infty \frac{\left(\tilde{b}(y)\right)^{\tilde{m}_v-k} e^{-\Delta(\tilde{b}(y))^2}}{2\sqrt{a}\bar{\sigma}^2} \Gamma\left(\frac{k+1}{2}, (\tilde{b}(y))^2\right) dy. \quad (67)$$

By substituting  $t = \tilde{b}(y)$  and invoking [23, 2.33.10],  $I_2$  can be derived as

$$I_2 = \frac{[(-1)^k + 1]\Gamma\left(\frac{k+1}{2}\right)}{2} \Gamma\left(\frac{\tilde{m}_v - k + 1}{2}, \Delta(\tilde{b}(r))^2\right). \quad (68)$$

By following manipulations similar to those in (62) and (64),  $J_2$  can be derived as

$$J_2 = (-1)^k \mathcal{J}(k, \tilde{b}(r)), \quad (69)$$

where  $\mathcal{J}(k, \tilde{b}(r))$  is defined in (16). By substituting (68) and (69) into (65),  $F_R(r)$  can be derived for  $r > \bar{\mu}$ . From probability theory, for  $\gamma = \bar{\gamma}R^2$  with  $\bar{\gamma} > 0, R > 0$ , we can write the PDF and CDF of  $\gamma$  as  $f_\gamma(y) = f_R(\sqrt{y/\bar{\gamma}})/(2\sqrt{y\bar{\gamma}})$  and  $F_\gamma(y) = F_R(\sqrt{y/\bar{\gamma}})$ , respectively [33]. By using this fact,  $F_\gamma(\cdot)$  can be written as (14).

#### APPENDIX C DERIVATION OF DIVERSITY ORDER IN (22) AND ASYMPTOTIC SER IN (33)

We notice that  $\tilde{W}_n = \eta_n \bar{g}_n \bar{h}_n$  is a scaled product of two Nakagami-m RVs. Hence, the PDF of  $\tilde{W}_n$  is given by [34]

$$f_{\tilde{W}_n}(\omega) = \psi_n \omega^{m_a+m_b-1} K_{m_a-m_b}(\omega\tau_n) \text{ for } \omega \geq 0, \quad (70)$$

where  $\psi_n = 4(m_a m_b)^{(m_a+m_b)/2} (\eta_n \sqrt{\kappa_a \kappa_b})^{-(m_a+m_b)/2} / (\Gamma(m_a)\Gamma(m_b))$  and  $\tau_n = 2\sqrt{m_a m_b / (\kappa_a \kappa_b \eta_n^2)}$ . In (70),  $K_v(\cdot)$  is the modified Bessel function of the second kind [23, 6.624.1]. The moment generating function (MGF) of  $\tilde{W}_n$  can be derived via [23, 6.621.3] as follows:

$$\mathcal{M}_{\tilde{W}_n}(s) = \psi'_n (s + \tau_n)^{-2m_a} \mathcal{F}(2m_a, m_a - m_b + 1/2; m_a + m_b + 1/2; s - \tau_n / (s + \tau_n)), \quad (71)$$

where  $\psi'_n = \sqrt{\pi} \psi_n (2\tau_n)^{m_a-m_b} \Gamma(2m_a) \Gamma(2m_b) / \Gamma(m_a + m_b + 1/2)$  and  $\mathcal{F}(\cdot, \cdot; \cdot; \cdot)$  is the hypergeometric function [23, 9.100]. Next, by utilizing the fact that  $\{\tilde{W}_1, \tilde{W}_2 \dots, \tilde{W}_n \dots, \tilde{W}_N\}$  are independent RVs, the MGF of  $\tilde{W} = \sum_{n=1}^N \tilde{W}_n$  can be derived as  $\mathcal{M}_{\tilde{W}}(s) = \prod_{n=1}^N \mathcal{M}_{\tilde{W}_n}(s)$  [24]. The order of smoothness of the PDF of  $\tilde{W}$  at the origin can be quantified by using the decaying order of the MGF  $\mathcal{M}_{\tilde{W}}(s)$  [27]. To this end, via the fact that  $(s - \tau_n)/(s + \tau_n) \rightarrow 1$  as  $s \rightarrow \infty$ , and since  $m_a < m_b$  satisfies the condition [23, 9.122.1] when  $s \rightarrow \infty$ ,  $\mathcal{M}_{\tilde{W}}(s)$  can be asymptotically approximated as

$$\mathcal{M}_{\tilde{W}}^\infty(s) = \left[ \prod_{n=1}^N \tilde{\psi}_n \right] s^{-2m_a N}, \quad (72)$$

where  $\tilde{\psi}_n = \psi_n \Gamma(m_a + m_b + 1/2) \Gamma(2m_b - 2m_1 - 1) / (\Gamma(m_b - m_a + 1/2) \Gamma(2m_b))$ .

Next, the behavior of the PDF of the SNR pertaining to the direct channel in high SNR regime is governed by the behavior of  $f_{\tilde{V}}(x)$  around  $x = 0$ . By substituting the Maclaurin series expansions of the exponential functions, the PDF can be approximated near the origin as  $f_{\tilde{V}}^{0+}(x) = \psi'_v x^{2m_v-1} + \mathcal{O}(x^{2m_v})$ , where  $\psi'_v = 2m_v^{m_v} / (\Gamma(m_v) \kappa_v^{m_v})$ . The corresponding MGF can be derived as [33]

$$\mathcal{M}_{\tilde{V}}^{\infty}(s) = \psi_v / (s^{2m_v}) \text{ and } \psi_v = \Gamma(2m_v) \psi'_v. \quad (73)$$

Since the direct and reflected channels via the IRS are independent RVs, the MGF of  $r = v + \tilde{W}$  when  $s \rightarrow \infty$  can be derived by using (72) and (73) as follows:

$$\mathcal{M}_R^{\infty}(s) = \mathcal{M}_{\tilde{V}}^{\infty}(s) \mathcal{M}_{\tilde{W}}^{\infty}(s) = \psi_v \left[ \prod_{n=1}^N \tilde{\psi}_n \right] / (s^{2m_v+2m_a N}). \quad (74)$$

By taking inverse Laplace transform of (74), the PDF of  $R$  can be approximated by a single polynomial term for  $r \rightarrow 0^+$  as

$$f_R^{0+}(r) = \Omega_R r^{2m_v+2m_a N-1} + \mathcal{O}(r^{2m_v+2m_a N}), \quad (75)$$

where  $\Omega_R = \psi_v \left[ \prod_{n=1}^N \tilde{\psi}_n \right] / \Gamma(2m_v + 2m_a N)$ . From (75), as  $\bar{\gamma} \rightarrow \infty$ , the CDF can be approximated at the origin as  $F_R^{0+}(r) = \int_0^r f_R^{0+}(t) dt$ . By performing the variable transformation  $r = \sqrt{y/\bar{\gamma}}$  [24], a single-polynomial asymptotic approximation of the CDF of  $\gamma$  is derived as

$$F_{\gamma}^{0+}(y) = \Omega_{op} (y/\bar{\gamma})^{G_d} + \mathcal{O}\left((y/\bar{\gamma})^{G_d+1}\right), \quad (76)$$

where  $G_d$  and  $\Omega_{op}$  are defined in (22) and (23), respectively. Then, the asymptotic outage probability and the diversity order can be derived as (21) and (22), respectively.

Next, the derivation of asymptotic average SER in the high SNR regime (33) is outlined. To begin with, the average SER can be written in an integral form as [35]

$$\bar{P}_e = \mathbb{E} \left[ \alpha \mathcal{Q} \left( \sqrt{\beta \bar{\gamma}} \right) \right] = \alpha \sqrt{\beta} / (2\sqrt{2\pi}) \int_0^{\infty} y^{-1/2} \exp(-\beta y/2) F_{\gamma}(y) dy \quad (77)$$

By substituting (76) into  $\bar{P}_e$  (77), an asymptotic average SER can be written as

$$\bar{P}_e^{\infty} = \frac{\alpha \sqrt{\beta} \Omega_{op}}{2\sqrt{2\pi} \bar{\gamma}^{G_d}} \int_0^{\infty} y^{G_d-1/2} \exp(-\beta y/2) dy. \quad (78)$$

By substituting  $t = \beta y/2$  into (78), and evaluating the integral via [23, Eqn. (8.310.1)], the asymptotic average SER in high SNR regime can be derived as (33).

APPENDIX D  
DERIVATION OF  $\mathcal{R}_{lb}$  IN (26),  $\mathcal{R}_{ub}$  IN (27), AND  $\mathcal{R}^\infty$  IN (29)

To begin with, the expectation term in (25) can be simplified as

$$\mathbb{E}[\gamma] = \bar{\gamma} \left( \mathbb{E}[\bar{v}^2] + 2\mathbb{E}[\bar{v}] \mathbb{E}[W] + \mathbb{E}[W^2] \right). \quad (79)$$

The RVs in (79) are distributed as  $\bar{v}^2 \sim \text{Gamma}(m_v, \kappa_v/m_v)$ ,  $\bar{v} \sim \text{Nakagami}(m_v, \kappa_v)$  and  $W \sim \mathcal{N}^+(\mu_W, \sigma_W^2)$ . Thus, the expectation terms in (79) can be derived as [33]

$$\mathbb{E}[\bar{v}^2] = \kappa_v, \quad \mathbb{E}[\bar{v}] = \frac{\Gamma(m_v + 1/2)}{\Gamma(m_v)} \left( \frac{\kappa_v}{m_v} \right)^{1/2}, \quad \mathbb{E}[W] = \mu_W, \quad \text{and} \quad \mathbb{E}[W^2] = \mu_W^2 + \sigma_W^2. \quad (80)$$

By substituting (80) into (79), and replacing  $\mathbb{E}[\gamma]$  in (25) with (79),  $\mathcal{R}_{ub}$  can be derived in closed-form as (27).

Next, we outline the derivation of a lower bound for the average achievable rate. To begin with, by applying the Taylor series expansion for  $1/\gamma$  around  $\mathbb{E}[\gamma]$ , the term  $\mathbb{E}[1/\gamma]$  in (25) can be approximated as [28]

$$\mathbb{E}[1/\gamma] \approx 1/\mathbb{E}[\gamma] + \mathbb{V}\text{ar}[\gamma]/(\mathbb{E}[\gamma])^3 = \mathbb{E}[\gamma^2]/(\mathbb{E}[\gamma])^3, \quad (81)$$

where  $\mathbb{E}[\gamma]$  is defined in (79) and  $\mathbb{E}[\gamma^2]$  is evaluated using  $\mathbb{E}[\gamma^2] = \bar{\gamma}^2 \mathbb{E}[(\bar{v} + W)^4]$ . Since  $\bar{v}$  and  $W$  are independent RVs, we have  $\mathbb{E}[(\bar{v} + W)^4] = \mathbb{E}[\bar{v}^4] + 4\mathbb{E}[\bar{v}^3] \mathbb{E}[W] + 6\mathbb{E}[\bar{v}^2] \mathbb{E}[W^2] + 4\mathbb{E}[\bar{v}] \mathbb{E}[W^3] + \mathbb{E}[W^4]$ . By using the fact that  $\bar{v}^2 \sim \text{Gamma}(m_v, \kappa_v/m_v)$  and invoking steps similar to those used in deriving (54),  $\mathbb{E}[\bar{v}^\alpha]$  for  $\alpha \in \{1, 2, 3, 4\}$  can be derived as  $\mathbb{E}[\bar{v}^\alpha] = \Gamma(m_v + \alpha/2) (\kappa_v/m_v)^{\alpha/2} / \Gamma(m_v)$ . Furthermore, by following mathematical manipulations that are used in deriving (57),  $\mathbb{E}[W^\alpha]$  for  $\alpha \in \{1, 2, 3, 4\}$  can be written as

$$\mathbb{E}[W^\alpha] = \frac{\xi}{2\sqrt{\pi}} \sum_{i=0}^{\alpha} \binom{\alpha}{i} \left( \sqrt{2\bar{\sigma}^2} \right)^i \bar{\mu}^{\alpha-i} \mathcal{I} \left( i, \frac{-\bar{\mu}}{\sqrt{2\bar{\sigma}^2}} \right), \quad (82)$$

where  $\mathcal{I}(\cdot, \cdot)$  is given in (17). By using  $\mathbb{E}[\bar{v}^\alpha]$  and  $\mathbb{E}[W^\alpha]$  for  $\alpha \in \{1, 2, 3, 4\}$ ,  $\mathbb{E}[(\bar{v} + W)^4]$  can be computed. Then, by substituting  $\mathbb{E}[\gamma]$  and  $\mathbb{E}[\gamma^2]$  into (81),  $\mathbb{E}[1/\gamma]$  can be computed. Thereby, by substituting  $\mathbb{E}[1/\gamma]$  into (25),  $\mathcal{R}_{lb}$  can be derived as in (26).

Next, the derivation of the asymptotic rate in (29) is outlined. By assuming  $\kappa_{g_n} = \kappa_g$ ,  $\kappa_{h_n} = \kappa_h$  and  $\eta_n = \eta \forall n$ , the variables  $\bar{\mu}$  and  $\bar{\sigma}^2$  can be simplified as  $\bar{\mu} = N\bar{\mu}_\infty$  and  $\bar{\sigma}^2 = N\bar{\sigma}_\infty^2$ , respectively, where  $\bar{\mu}_\infty$  and  $\bar{\sigma}_\infty^2$  can be written as  $\bar{\mu}_\infty = \eta \sqrt{\kappa_g \kappa_h / m_g m_h T(m_g, m_h, 1/2)}$ , and  $\bar{\sigma}_\infty^2 = \eta^2 \kappa_g \kappa_h (1 - T^2(m_g, m_h, 1/2) / m_g m_h)$ . When  $N \rightarrow \infty$ , the SNR (26) can be derived as

$$\lim_{N \rightarrow \infty} \gamma_{lb} = \lim_{N \rightarrow \infty} \frac{\bar{\gamma} N^2 \left( \frac{\kappa_v}{N^2} + 2 \frac{\mu_W}{N^2} \Gamma(m_v + 1/2) \sqrt{\kappa_v/m_v} / \Gamma(m_v) + \frac{\mu_W^2}{N^2} + \frac{\sigma_W^2}{N^2} \right)^3}{\left( \frac{\xi}{2\sqrt{\pi}} \bar{\mu}_\infty^4 \mathcal{I} \left( 0, \frac{-\sqrt{N}\bar{\mu}_\infty}{\sqrt{2\bar{\sigma}_\infty^2}} \right) + \frac{\Lambda(N)}{N^4} \right)} \stackrel{(a)}{=} \bar{\gamma}_E \bar{\mu}_\infty^2, \quad (83)$$

where  $\bar{\gamma}_E = \lim_{N \rightarrow \infty} \bar{\gamma}/N^2$ ,  $\mathcal{I}(\cdot, \cdot)$  is defined in (17),  $\Lambda(N)$  is a polynomial of order 3 and it captures the remaining terms of the expansion of the denominator of  $\gamma_{lb}$ . The limits in step (a) of (83) are evaluated by invoking (11),  $\lim_{N \rightarrow \infty} \xi = 1$ ,  $\lim_{N \rightarrow \infty} \mathcal{I}\left(0, -\sqrt{N}\bar{\mu}_\infty/\sqrt{2\bar{\sigma}_\infty^2}\right) = \mathcal{I}(0, -\infty) = 2\gamma(1/2)$  and  $\lim_{N \rightarrow \infty} \mu_W^2/N^2 = \bar{\mu}_\infty^2$ . Similarly, in the asymptotic regime, the SNR term in  $\mathcal{R}_{ub}$  (27) can be derived as

$$\lim_{N \rightarrow \infty} \gamma_{ub} = \lim_{N \rightarrow \infty} \bar{\gamma}N^2 \left( \frac{\kappa_v}{N^2} + 2\frac{\mu_W}{N^2} \Gamma(m_v + 1/2) \sqrt{\kappa_v/m_v} / \Gamma(m_v) + \frac{\mu_W^2}{N^2} + \frac{\sigma_W^2}{N^2} \right) = \bar{\gamma}_E \bar{\mu}_\infty^2. \quad (84)$$

Thus, we have  $\lim_{N \rightarrow \infty} \mathcal{R}_{lb} = \lim_{N \rightarrow \infty} \mathcal{R}_{ub} = \log(1 + \bar{\gamma}_E \bar{\mu}_\infty^2)$ , which can be rewritten as (29).

#### APPENDIX E THE DERIVATION OF THE AVERAGE SER IN (31)

To begin with,  $\bar{P}_e$  in (30) can be alternatively written as

$$\bar{P}_e \approx \alpha \int_0^\infty \int_0^\infty \mathcal{Q}\left(\sqrt{\beta\bar{\gamma}}(x+w)\right) f_{\bar{v}}(x) f_W(w) dx dw, \quad (85)$$

where  $f_{\bar{v}}(x)$  and  $f_W(w)$  are given in (1) and (7), respectively. The  $\mathcal{Q}$ -function,  $\mathcal{Q}(\sqrt{\beta\bar{\gamma}}(x+w))$ , in (85) can be alternatively written as [23]

$$\mathcal{Q}\left(\sqrt{\beta\bar{\gamma}}(x+w)\right) = \frac{1}{\pi} \int_0^{\pi/2} \exp\left(-\frac{\beta\bar{\gamma}x^2}{2\sin^2\vartheta} - \frac{\beta\bar{\gamma}y^2}{2\cos^2\vartheta}\right) d\vartheta. \quad (86)$$

By substituting (86) into (85) and by applying several mathematical manipulations, we have

$$\bar{P}_e \approx \tilde{\mathcal{U}} \int_0^{\pi/2} \mathcal{I}_{\bar{v}}(\vartheta) \mathcal{I}_W(\vartheta) d\vartheta, \quad (87)$$

where  $\tilde{\mathcal{U}} = 2m_v^{m_v} \xi e^{-\bar{\mu}^2/2\bar{\sigma}^2} / \left(\sqrt{2\pi\bar{\sigma}^2} \Gamma(m_v) \kappa_v^{m_v} \pi\right)$ . In (87),  $\mathcal{I}_{\bar{v}}(\vartheta)$  and  $\mathcal{I}_W(\vartheta)$  are defined as

$$\mathcal{I}_{\bar{v}}(\vartheta) = \int_0^\infty x^{2m_v-1} e^{-u_1 x^2} dx \quad \text{and} \quad \mathcal{I}_W(\vartheta) = \int_0^\infty e^{-(z_1 y^2 + 2z_2 y)} dy, \quad (88)$$

where  $u_1 = (m_v/\kappa_v + \beta\bar{\gamma}/(2\sin^2(\vartheta)))$ ,  $z_1 = (1/2\bar{\sigma}^2 + \beta\bar{\gamma}/(2\cos^2(\vartheta)))$  and  $z_2 = \bar{\mu}/2\bar{\sigma}^2$ . By substituting  $t = \sqrt{u_1}x$  and using the definition of Gamma function,  $\mathcal{I}_{\bar{v}}(\vartheta)$  can be evaluated as

$$\mathcal{I}_{\bar{v}}(\vartheta) = \frac{1}{2u_1^{m_v}} \int_0^\infty t^{m_v-1} e^{-t} dt = \frac{\Gamma(m_v)}{2} \left[ \frac{m_v}{\kappa_v} + \frac{\beta\bar{\gamma}}{(2\sin^2(\vartheta))} \right]^{-m_v}. \quad (89)$$

By invoking [23, 2.33.1],  $\mathcal{I}_W(\vartheta)$  can be derived as

$$\mathcal{I}_W(\vartheta) = 2 \sqrt{\frac{\pi}{\left(\frac{1}{2\bar{\sigma}^2} + \frac{\beta\bar{\gamma}}{2\cos^2(\vartheta)}\right)}} \exp\left(\frac{\bar{\mu}^2/4\bar{\sigma}^4}{\left(\frac{1}{2\bar{\sigma}^2} + \frac{\beta\bar{\gamma}}{2\cos^2(\vartheta)}\right)}\right) \mathcal{Q}\left(-\frac{\sqrt{2}\bar{\mu}}{1 + \frac{\beta\bar{\gamma}\bar{\sigma}^2}{\cos^2(\vartheta)}}\right). \quad (90)$$

By substituting (89) and (90) into (87),  $\bar{P}_e$  can be alternatively written as

$$\bar{P}_e \approx \mathcal{U} \int_0^{\pi/2} \frac{\exp\left(\bar{\mu}^2 / \left(2\bar{\sigma}^2 + \frac{2\beta\bar{\gamma}\bar{\sigma}^4}{\cos^2(\vartheta)}\right)\right)}{\left[\frac{m_v}{\kappa_v} + \frac{\beta\bar{\gamma}}{(2\sin^2(\vartheta))}\right]^{m_v} \sqrt{\left(\frac{1}{2\bar{\sigma}^2} + \frac{\beta\bar{\gamma}}{2\cos^2(\vartheta)}\right)}} \mathcal{Q}\left(-\frac{\sqrt{2}\bar{\mu}}{1 + \frac{\beta\bar{\gamma}\bar{\sigma}^2}{\cos^2(\vartheta)}}\right) d\vartheta, \quad (91)$$

where  $\mathcal{U} = \Gamma(m_v)\sqrt{\pi}\tilde{\mathcal{U}}$ . Let  $\mathcal{P}(\vartheta)$  be the integrand of (91), and then,  $\vartheta_u$  in (32) provides the argument that maximizes  $\mathcal{P}(\vartheta)$ . Therefore, the integral in (91) can be upper bounded as

$$\int_0^{\pi/2} \mathcal{P}(\vartheta) d\vartheta \leq \pi \mathcal{P}(\vartheta_u)/2. \quad (92)$$

By replacing the integral in (91) by (92), the desired upper bound can be derived as in (31).

## REFERENCES

- [1] D. P. Kudathanthirige, D. Gunasinghe, and G. L. A. Aruma Baduge, “Performance Analysis of Intelligent Reflective Surfaces for Wireless Communication,” in *Proc. IEEE Int. Conf. Commun. (ICC)*, Jun. 2020.
- [2] C. Liaskos *et al.*, “A New Wireless Communication Paradigm through Software-Controlled Metasurfaces,” *IEEE Commun. Mag.*, vol. 56, no. 9, pp. 162–169, Sep. 2018.
- [3] M. Di Renzo *et al.*, “Smart radio environments empowered by reconfigurable AI meta-surfaces: An idea whose time has come,” *EURASIP J. Wireless Commun. Net.*, no. 129, May 2019.
- [4] S. H. Lee *et al.*, “Switching Terahertz Waves with Gate-Controlled Active Graphene Metamaterials,” *Nature Materials*, vol. 11, no. 11, pp. 936–941, 2012.
- [5] Q. Wu and R. Zhang, “Intelligent Reflecting Surface Enhanced Wireless Network via Joint Active and Passive Beamforming,” *IEEE Trans. Wireless Commun.*, vol. 18, no. 11, pp. 5394–5409, Nov. 2019.
- [6] E. Basar *et al.*, “Wireless Communications Through Reconfigurable Intelligent Surfaces,” *IEEE Access*, vol. 7, pp. 116 753–116 773, Aug. 2019.
- [7] Y. Han, W. Tang, S. Jin, C. Wen, and X. Ma, “Large Intelligent Surface-Assisted Wireless Communication Exploiting Statistical CSI,” *IEEE Trans. Veh. Technol.*, vol. 68, no. 8, pp. 8238–8242, Aug 2019.
- [8] J. Chen, Y. Liang, Y. Pei, and H. Guo, “Intelligent Reflecting Surface: A Programmable Wireless Environment for Physical Layer Security,” *IEEE Access*, vol. 7, pp. 82 599–82 612, 2019.
- [9] H. Zhang, B. Di, L. Song, and Z. Han, “Reconfigurable Intelligent Surfaces Assisted Communications With Limited Phase Shifts: How Many Phase Shifts Are Enough?” *IEEE Trans. Veh. Technol.*, vol. 69, no. 4, pp. 4498–4502, April 2020.
- [10] S. Abeywickrama, R. Zhang, Q. Wu, and C. Yuen, “Intelligent reflecting surface: Practical phase shift model and beamforming optimization,” *IEEE Trans. Commun.*, 2020, accepted.
- [11] M. Jung, W. Saad, Y. Jang, G. Kong, and S. Choi, “Performance Analysis of Large Intelligent Surfaces (LISs): Asymptotic Data Rate and Channel Hardening Effects,” *IEEE Trans. Wireless Commun.*, vol. 19, no. 3, pp. 2052–2065, 2020.
- [12] Q.-U.-A. Nadeem, A. Kammoun, A. Chaaban, M. Debbah, and M.-S. Alouini, “Asymptotic Max-Min SINR Analysis of Reconfigurable Intelligent Surface Assisted MISO Systems,” *arXiv:1903.08127*, 2019.
- [13] Z. Zhang, Y. Cui, F. Yang, and L. Ding, “Analysis and Optimization of Outage Probability in Multi-Intelligent Reflecting Surface-Assisted Systems,” *arXiv:1909.02193*, 2019.
- [14] M. Jung, W. Saad, Y. Jang, G. Kong, and S. Choi, “Reliability Analysis of Large Intelligent Surfaces (LISs): Rate Distribution and Outage Probability,” *IEEE Wireless Commun. Lett.*, vol. 8, no. 6, pp. 1662–1666, 2019.
- [15] M. Badiu and J. P. Coon, “Communication Through a Large Reflecting Surface With Phase Errors,” *IEEE Wireless Commun. Lett.*, vol. 9, no. 2, pp. 184–188, 2020.
- [16] C. Psomas and I. Krikidis, “Low-Complexity Random Rotation-based Schemes for Intelligent Reflecting Surfaces,” *arXiv:1912.10347*, 2019.

- [17] C. Guo, Y. Cui, F. Yang, and L. Ding, "Outage Probability Analysis and Minimization in Intelligent Reflecting Surface-Assisted MISO Systems," *IEEE Commun. Lett.*, 2020, IEEE Early Access.
- [18] E. Basar and I. F. Akyildiz, "Reconfigurable Intelligent Surfaces for Doppler Effect and Multipath Fading Mitigation," *arXiv:1912.04080*, 2019.
- [19] S. Hu and F. Rusek, "Spherical Large Intelligent Surfaces," in *Proc IEEE International Conference on Acoustics, Speech and Signal Processing (ICASSP)*, Barcelona, Spain, May 2020, pp. 8673–8677.
- [20] S. Zhang and R. Zhang, "Intelligent Reflecting Surface Aided Multiple Access: Capacity Region and Deployment Strategy," *arXiv:2002.07091*, 2020.
- [21] D. L. Galappaththige, D. Kudathanthirige, and G. Amarasuriya Aruma Baduge, "Performance Analysis of Distributed Intelligent Reflective Surface Aided Communications," in *IEEE Global Communications Conference (GLOBECOM)*, May 2020, pp. 1–6, (submitted).
- [22] G. L. Stüber, *Principles of Mobile Communication*. Springer, 2017.
- [23] I. Gradshteyn and I. Ryzhik, *Table of integrals, Series, and Products*, 7th ed. Academic Press, 2007.
- [24] A. Papoulis and S. Unnikrishna Pillai, *Probability, Random Variables and Stochastic Processes*. McGraw-Hill Europe, 4th edition, 2002.
- [25] M. D. Renzo *et al.*, "Towards Smart and Reconfigurable Environment: Intelligent Reflecting Surface Aided Wireless Network," *EURASIP J. Wireless Commun. Net.*, May 2019.
- [26] Q. Wu and R. Zhang, "Towards Smart and Reconfigurable Environment: Intelligent Reflecting Surface Aided Wireless Network," *IEEE Commun. Mag.*, vol. 58, no. 1, pp. 106–112, 2020.
- [27] Z. Wang and G. B. Giannakis, "A simple and general parameterization quantifying performance in fading channels," *IEEE Trans. Commun.*, vol. 51, no. 8, pp. 1389–1398, Aug. 2003.
- [28] Q. Zhang, S. Jin, K.-K. Wong, H. Zhu, and M. Matthaiou, "Power Scaling of Uplink Massive MIMO Systems With Arbitrary-Rank Channel Means," *IEEE J. Sel. Areas Commun.*, vol. 8, no. 5, pp. 966–981, Oct. 2014.
- [29] J. Proakis and M. Salehi, *Digital Communications*. McGraw-Hill Education, 5th edition, 2007.
- [30] A. Goldsmith, *Wireless Communications*. Cambridge University Press, 2005.
- [31] Haykin and Moher, *Communication Systems*. John Wiley & Sons, Inc., 5th edition, 2009.
- [32] D. P. Kudathanthirige and G. A. Aruma Baduge, "Multi-User Massive MIMO Relay Networks With Space-Constrained 2-D Antenna Arrays," *IEEE Commun. Lett.*, vol. 21, no. 11, pp. 2540–2543, 2017.
- [33] A. Papoulis and S. U. Pillai, *Probability, Random Variables, and Stochastic Processes*, 4th ed. McGraw Hill, 2002.
- [34] G. K. Karagiannidis, N. C. Sagias, and P. T. Mathiopoulos, "N\*Nakagami: A Novel Stochastic Model for Cascaded Fading Channels," *IEEE Trans. Commun.*, vol. 55, no. 8, pp. 1453–1458, 2007.
- [35] G. Amarasuriya, C. Tellambura, and M. Ardakani, "Performance Analysis of Transmit Antenna Selection Strategies for Cooperative MIMO AF Relay Networks," *IEEE Trans. Veh. Technol.*, vol. 60, no. 7, pp. 3030–3044, 2011.